2012

Spontaneous activity promotes synapse formation in a cell-type-dependent manner in the developing retina

Florentina Soto
Washington University School of Medicine in St. Louis

Xiaofeng Ma
Washington University School of Medicine in St. Louis

Jacob L. Cecil
Washington University School of Medicine in St. Louis

Bradly Q. Vo
Washington University School of Medicine in St. Louis

Susan M. Culican
Washington University School of Medicine in St. Louis

See next page for additional authors

Development/Plasticity/Repair

Spontaneous Activity Promotes Synapse Formation in a Cell-Type-Dependent Manner in the Developing Retina

Florentina Soto,[1] Xiaofeng Ma,[1] Jacob L. Cecil,[1] Bradly Q. Vo,[1] Susan M. Culican,[1] and Daniel Kerschensteiner[1,2]
Departments of [1]Ophthalmology and Visual Sciences and [2]Anatomy and Neurobiology, Washington University School of Medicine, St. Louis, Missouri 63110

Spontaneous activity is thought to regulate synaptogenesis in many parts of the developing nervous system. *In vivo* evidence for this regulation, however, is scarce and comes almost exclusively from experiments in which normal activity was reduced or blocked completely. Thus, whether spontaneous activity itself promotes synaptogenesis or plays a purely permissive role remains uncertain. In addition, how activity influences synapse dynamics to shape connectivity and whether its effects among neurons are uniform or cell-type-dependent is unclear. In mice lacking the cone–rod homeobox gene (*Crx*), photoreceptors fail to establish normal connections with bipolar cells (BCs). Here, we find that retinal ganglion cells (RGCs) in $Crx^{-/-}$ mice become rhythmically hyperactive around the time of eye opening as a result of increased spontaneous glutamate release from BCs. This elevated neurotransmission enhances synaptogenesis between BCs and RGCs, without altering the overall circuit architecture. Using live imaging, we discover that spontaneous activity selectively regulates the rate of synapse formation, not elimination, in this circuit. Reconstructions of the connectivity patterns of three BC types with a shared RGC target further revealed that neurotransmission specifically promotes the formation of multisynaptic appositions from one BC type without affecting the maintenance or elimination of connections from the other two. Although hyperactivity in $Crx^{-/-}$ mice persists, synapse numbers do not increase beyond 4 weeks of age, suggesting closure of a critical period for synaptic refinement in the inner retina. Interestingly, despite their hyperactivity, RGC axons maintain normal eye-specific territories and cell-type-specific layers in the dorsal lateral geniculate nucleus.

Introduction

Spontaneous activity transmitted among developing neurons is thought to shape the connectivity patterns of emerging circuits. The precise role of spontaneous activity during synaptogenesis, however, remains unclear (Katz and Shatz, 1996). Nearly all studies so far have probed this relationship using manipulations that suppress or abolish normal activity (Bleckert and Wong, 2011). A frequent finding among these studies has been that silenced circuits develop fewer synapses (Okabe et al., 1999; Bouwman et al., 2004; Ultanir et al., 2007; Kerschensteiner et al., 2009). This may reflect a purely permissive function of activity, which is required for neurons to correctly present and respond to molecular cues that define the numbers and patterns of synapses. Alternatively, spontaneous activity could itself promote synaptogenesis and differentially regulate the emergence of distinct connectivity patterns. This would predict that elevating spontaneous activity in developing circuits should raise the number of synapses above normal levels.

Synaptogenesis in most neural circuits is a high turnover process in which many synapses are short-lived (Alsina et al., 2001; Niell et al., 2004; Kerschensteiner et al., 2009). Therefore, activity could, in principle, shape connectivity by regulating synapse formation, elimination, or both. Few studies have directly analyzed the influence of spontaneous activity on synapse dynamics in developing circuits. At the neuromuscular junction, inhibition of acetylcholine synthesis in a subset of motor neurons or local blockade of postsynaptic receptors promotes synapse elimination (Balice-Gordon and Lichtman, 1994; Buffelli et al., 2003). In contrast, reduced glutamate release from BC axons in the retina selectively lowers the rate of synapse formation with their targets (Kerschensteiner et al., 2009). In cultured neurons, decreases in both synapse formation and elimination have been observed after pharmacologic blockade of activity (Okabe et al., 1999).

To harness spontaneous activity and establish specific wiring patterns, developing circuits need to have boundaries in place that restrict the influence of activity on synaptic development. We currently know little about these boundaries. For example, whether the effects of activity on synaptogenesis in a given circuit are uniform or cell-type dependent is unclear (Morgan et al., 2011). Similarly, the critical developmental periods during which spontaneous activity most effectively regulates synaptogenesis for many circuits have not been identified (Hensch, 2004).

Here, we report that, in $Crx^{-/-}$ mice, spontaneous glutamate release from bipolar cells (BCs) is elevated and BC–retinal ganglion cell (RGC) synaptogenesis is increased. This effect is medi-

Received Jan. 13, 2012; revised Feb. 20, 2012; accepted Feb. 25, 2012.

Author contributions: F.S. and D.K. designed research; F.S., X.M., J.L.C., B.Q.V., S.M.C., and D.K. performed research; F.S., X.M., J.L.C., B.Q.V., S.M.C., and D.K. analyzed data; F.S. and D.K. wrote the paper.

This work was supported by the Hope for Vision Foundation (D.K.), the Edward Mallinckrodt Jr. Foundation (D.K.), the Alfred P. Sloan Foundation (D.K.), the Whitehall Foundation (D.K.), National Institutes of Health Grants R01 EY021855 (D.K.), K12 EY016336 (S.M.C.), and P30 EY0268 (Department of Ophthalmology and Visual Sciences at Washington University), and a Research to Prevent Blindness unrestricted grant (Department of Ophthalmology and Visual Sciences at Washington University). We thank Drs. C. L. Cepko, S. Chen, J. C. Corbo, and A. D. Huberman for mice and members of the Kerschensteiner laboratory for comments on this manuscript.

Correspondence should be addressed to Daniel Kerschensteiner, Department of Ophthalmology and Visual Sciences, Washington University School of Medicine, 660 South Euclid Avenue, St. Louis, MO 63110. E-mail: dkerschensteiner@wustl.edu.

DOI:10.1523/JNEUROSCI.0194-12.2012

 0270-6474/12/325426-14$15.00/0

ated by selective changes in synapse formation, not elimination, and is expressed in a cell-type-dependent manner among converging BCs. We find that synaptic patterns in $Crx^{-/-}$ retinas stabilize by 4 weeks of age despite continued hyperactivity, likely indicating the closure of a critical period, and analyze the projection patterns of RGC axons. $Crx^{-/-}$ mice are a model of Leber's congenital amaurosis (LCA), a cone–rod dystrophy affecting ~20% of children enrolled in schools for the blind (Damji et al., 2001). Knowledge of the changes in synaptic development in $Crx^{-/-}$ retinas might help inform the design of vision rescue strategies for patients with LCA.

Materials and Methods

Animals. Throughout this study, we compared mice of either sex lacking the cone–rod homeobox gene *Crx* in a mixed 129SVJ/C57BL/J6 background ($Crx^{-/-}$) to wild-type (WT) littermates. In some instances, results from WT mice in a pure C57BL/J6 background were included after verifying that they were indistinguishable from those obtained in the 129SVJ/C57BL/J6 background. *Grm6–tdTomato* and *DRD4–GFP* mice were crossed to $Crx^{-/-}$ mice to reconstruct the patterns of synapses between BCs and RGCs and visualize mosaics and retinofugal projections of direction-selective ganglion cells (DSGCs), respectively (Huberman et al., 2009; Kerschensteiner et al., 2009). Both transgenic mouse lines were backcrossed to C57BL/6 for more than six generations before mating to $Crx^{-/-}$ mice.

Tissue preparation. For multielectrode array and patch-clamp recordings, mice were dark adapted for ~2 h. Eyes were removed from mice deeply anesthetized with CO_2 and prepared as either cups by removing the cornea, lens, and vitreous or as flat mounts on membrane discs (Millipore) by further isolating the retina from the sclera and pigment epithelium. All procedures were approved by the Animal Studies Committee of Washington University School of Medicine and were performed in compliance with the National Institutes of Health *Guide for the Care and Use of Laboratory Animals.* Eye cups and isolated retinas were stored in a light-tight chamber at ~33°C in bicarbonate (multielectrode array recordings, patch-clamp recordings) or HEPES-buffered (biolistics, live imaging) mouse artificial CSF (mACSF). For immunohistochemistry, eye cups and isolated retinas were fixed in 4% paraformaldehyde (PFA) in mACSF for 30 min at room temperature. To analyze RGC projections to the brain, mice were deeply anesthetized with sodium pentobarbital and transcardially perfused with 4% PFA in PBS. Brains were then removed and postfixed for 3 h in 4% PFA in PBS at 4°C.

Intraocular injections. Mice were anesthetized with a mixture of ketamine (100 μg/mg) and xylazine (10 μg/mg). One to 2 μl of β-cholera toxin conjugated to Alexa Fluor 488 or Alexa Fluor 594 (1 mg/ml in PBS) were injected into each eye. Cholera toxin was allowed to be anterogradely transported for 1–2 d before mice were killed. Only brains in which dorsal lateral geniculate nuclei (dLGNs) were completely outlined by signal of the fluorophore injected in the contralateral eye were included in our analysis.

Immunohistochemistry. Vibratome sections (brain or eye cup) and retinal flat mounts were incubated with primary antibodies against calbindin (1:1000; Synaptic Systems), calretinin (1:1000; Millipore), choline acetyltransferase (ChAT; 1:100), C-terminal binding protein 2 (CtBP2; 1:1000; BD Biosciences), protein kinase Cα, (PKCα; 1:1000; Sigma), rhodopsin (1:400; Millipore), synaptotagmin 2 (SytII or Znp-1; 1:1000; Zebrafish International Resource Center), vesicular glutamate transporter 1 (VGluT1; 1:1000; Millipore), vesicular glutamate transporter 3 (VGluT3; 1:1000; Millipore), and voltage-gated L-type calcium channel α-subunit 1S (CACNA1S; 1:1000; Millipore Bioscience Research Reagents) for 2–7 d at 4°C, washed, and incubated with secondary antibodies (Alexa Fluor 488, 568, or 633 conjugates; 1:1000; Invitrogen) overnight at 4°C.

Biolistic transfection. Plasmids driving expression of tandem dimer Tomato (tdTomato), cyan fluorescent protein (CFP), and postsynaptic density protein 95 fused to yellow or cyan fluorescent protein (PSD95–Y/CFP) from a cytomegalovirus promoter were precipitated onto gold particles (12.5 mg, 1.6 μm diameter; Bio-Rad) as described previously (Morgan and Kerschensteiner, 2012). A Helios Gene gun (Bio-Rad) was used to deliver gold particles (~40 psi) to RGCs in flat-mount preparations (Morgan and Kerschensteiner, 2011). The tissue was then incubated for 12–18 h in a humid, warm (~33°C), and oxygenated chamber in HEPES-buffered mACSF before fixation in 4% PFA. HEPES-buffered mACSF contained the following (in mM): 119 NaCl, 2.5 KCl, 2.5 $CaCl_2$, 1.3 $MgCl_2$, 1 NaH_2PO_4, 11 glucose, and 20 HEPES. The pH was adjusted to 7.37 with NaOH.

Image acquisition and analysis. Images were acquired on an Olympus Fv1000 laser scanning confocal microscope using 60×, 1.35 NA (fixed retina) and 20×, 0.85 NA (brain) oil-immersion objectives or a 60×, 1.1 NA (live retina) water-immersion objective. Voxel sizes of image stacks were 0.069–0.069–0.3 μm (*x–y–z*, live retina), 0.103–0.103–0.3 μm (*x–y–z*, fixed retina), or 0.309–0.309–0.5 μm (*x–y–z*, brain). Images were processed and analyzed using NIH ImageJ, Amira (Visage Imaging), and software written in Matlab (MathWorks).

To identify the positions of labeled somata and analyze their distribution, *z*-projections of confocal image stacks were binarized into soma and non-soma pixels using Otsu's method for thresholding (Otsu, 1979), followed by a size filter. Next, the binary image was transformed into a distance map, in which the value of each pixel reflects its distance from the nearest non-soma pixel. The centers of mass of the regional maxima (i.e., connected pixels of equal value that are surrounded by pixels of lower value) in the distance image then were defined as the soma positions. This algorithm reliably identified the positions of somata even when their boundaries overlapped. To characterize the regularity of soma positions in the inner retina, we analyzed the distribution of nearest-neighbor distances and the density recovery profile (Rodieck, 1991). In the density recovery profile, the density of neurons of a specific type is calculated at increasing distances from a reference cell. Each cell in a field of view is once the reference cell, and observed densities are normalized by the area included in the respective distance bin. A dip in the density recovery profile close to the origin indicates an exclusion zone, the extent of which is quantified as an effective radius (i.e., the radius of a cylinder with equal volume to the dip in a 3D density recovery profile plot).

Branching patterns of RGC dendrites and distributions of excitatory synapses on them were reconstructed as described previously (Morgan et al., 2008; Kerschensteiner et al., 2009). Briefly, dendritic skeletons consisting of linked ~1-μm-long segments were generated from binary masks (Amira) based on the cytosolic fluorescent signal of RGCs. The area covered by the dendrite was computed by convolving a *z*-projection of the dendritic skeleton with a 10-μm-diameter circle mimicking BC axon terminals. The density of dendritic branching was defined as the length of the dendritic skeleton divided by the area it covers. Stratification of RGC dendrites was measured by the SD of the *z*-positions of skeleton segments. To prevent slants in the tissue from biasing stratification measures, for each segment, the SD of the *z*-positions of segments within 30 μm in *x–y* was calculated. The stratification index of an RGC dendrite was then defined as the average SD across all its segments. BC synapses on RGC dendrites were identified by a previously described algorithm involving the following: iterative thresholding of the PSD95–Y/CFP signal, size filtering, an estimation of the deviation of the synaptic signal from a linear prediction based on the signal of the cytosolic fluorophore, and a final user-guided stage of error minimization (Morgan et al., 2008; Kerschensteiner et al., 2009).

For live imaging of synaptogenesis, retinal flat-mount preparations were continuously perfused with 1–2 ml/min of warm (~33°C) HEPES-buffered mACSF. Image stacks were acquired every 2 h for up to 12 h. For analysis, image stacks were median-filtered, PSD95–Y/CFP puncta identified by eye, and manually tracked through the time series (Kerschensteiner et al., 2009; Morgan et al., 2011).

Connectivity patterns of pairs of BCs and RGCs were analyzed as described previously (Morgan et al., 2011). Pairs consisted of type 10 RGCs (G10) labeled biolistically with CFP and PSD95–YFP and one of three types of BCs [type 6 (B6), type 7 (B7), and rod bipolar (RB)] labeled in *Grm6–tdTomato* mice. BC and RGC types were identified based on their characteristic morphologies (Ghosh et al., 2004; Völgyi et al., 2009). Because the number of synapses of one BC with an RGC is low (typically <15) compared with the total number of excitatory synapses on an RGC dendrite (~1500), it was feasible to count connections manually by inspecting image stacks plane by plane. To be assigned to a cell pair, syn-

apses (i.e., PSD95–YFP puncta) had to occur at regions where the axonal and dendritic fluorescence overlapped (i.e., axo-dendritic appositions). On a subset of the data, BC axons and RGC dendrites were masked by applying isointensity thresholds (Amira) to the respective image channels. Axo-dendritic appositions were then defined as regions of >50 connected voxels shared between axonal and dendritic masks. Appositions identified in this analysis matched >95% of the appositions identified by eye. Finally, although optical resolution limits the certainty with which we can determine contact between axons and dendrites, the large size of BC axonal boutons makes it very unlikely that synapses were wrongly assigned to a given BC.

To analyze the segregation of RGC axons from the ipsilateral and contralateral eye, *R* values of image pixels from the dLGN were calculated according to Torborg and Feller (2004):

$$R = \log_{10}(F_I/F_C),$$

where F_I and F_C refer to the fluorescence of axons from the ipsilateral and contralateral eyes, respectively. Segregation was measured as the variance of *R* values across the dLGN.

Multielectrode array recordings and analysis. Action potentials from RGCs were recorded on planar arrays of 252 electrodes (30 μm electrode size, 100 μm electrode spacing) arranged in a 16 × 16 grid with the four corners left empty (MultiChannelSystems). Rectangular pieces of isolated retina were mounted on the arrays RGC-side down and secured by a transparent tissue culture membrane (3 μm pore size; Corning) weighed down by a platinum ring (Kerschensteiner et al., 2008). The tissue was perfused at a rate of 1–2 ml/min with warm (~33°C) bicarbonate-buffered mACSF containing the following (in mM): 125 NaCl, 2.5 KCl, 1 $MgCl_2$, 1.25 NaH_2PO_4, 2 $CaCl_2$, 20 glucose, and 26 $NaHCO_3$ (equilibrated with 95% O_2/5% CO_2). Signals of each electrode were bandpass filtered between 300 and 3000 Hz and digitized at 5 kHz. Signal cutouts from 1 ms before to 2 ms after crossings of negative thresholds (set manually for each channel) were recorded to hard disk together with the time of threshold crossing (i.e., spike time). Principal component analysis of these waveforms was used to sort spikes into trains representing the activity of individual neurons (Offline Sorter; Plexon). Refractory periods in spike trains were used to assess the quality of the sorting, and only spike trains in which <0.2% of interspike intervals were <2 ms were retained. Cross-correlations among spike trains were used to detect when activity from a single neuron had been recorded on more than one electrode. In these cases, only the train with the most spikes was used for additional analysis.

Correlation indices (i.e., the factor by which the firing of cell Y increases above its average rate in a time window Δt around spikes in cell X) were calculated following a previous definition (Wong et al., 1993) as follows:

$$CI_{XY} = \frac{N_{XY}(-\Delta t, +\Delta t) \times T}{N_{X(O,T)} \times N_{Y(O,T)} \times 2\Delta t} \quad (2)$$

where N_{XY} is the number of spikes cell Y fired within $\pm\Delta t$ (set to 0.1 s) from spikes in cell X, *T* is the total length of the recording, and N_X and N_Y signify the total number of spikes of cells X and Y, respectively, during the recording.

Power spectral densities of RGC spike trains or synaptic input currents to RGCs were calculated from the fast Fourier transforms of the respective autocorrelation functions using Neuroexplorer (Nex Technologies) and Matlab.

Patch-clamp recordings and analysis. We performed whole-cell voltage-clamp recordings from RGCs in flat-mount preparations using pipettes (4–7 MΩ, borosilicate glass) filled with the following (in mM): 120 Cs-gluconate, 1 $CaCl_2$, 1 $MgCl_2$, 10 Na-HEPES, 11 EGTA, 10 TEA-Cl, and 2 QX-314, pH adjusted to 7.2 with CsOH. Internal solution included 0.1 mM of either Alexa Fluor 488 or Alexa Fluor 568. Retinas were perfused at a rate of 2–3 ml/min with warm (~33°C) bicarbonate-buffered mACSF (equilibrated with 95% O_2/5% CO_2). To restrict recordings to large monostratified RGC types included in the analysis of connectivity patterns, cells with large somata (~20 μm) were targeted under infrared illumination. At the end of each recording, dendrites were visualized using two-photon laser scanning microscopy to confirm cell-type identification. Patch-clamp data were acquired using a Multiclamp 700B amplifier, low-pass filtered at 2 kHz, and digitized at 10 kHZ. The junction potential of ~12 mV was corrected offline. Series resistance (~15 MΩ) was compensated electronically by ~75%. To record EPSCs, RGCs were voltage clamped at the reversal potential of chloride-mediated currents (E_{Cl} = −60 mV). To analyze input levels, the charge transfer was measured by integrating a 30 s segment of each EPSC trace.

Statistics. Unless noted otherwise, Wilcoxon–Mann–Whitney rank sum tests were used to assess statistical significance of differences between groups.

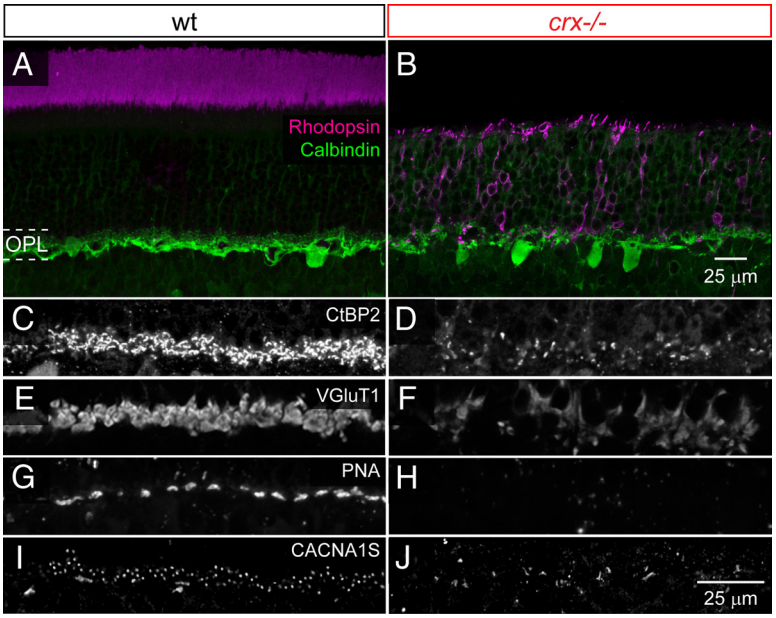

Figure 1. Presynaptic and postsynaptic specializations are disrupted in the OPL of $Crx^{-/-}$ mice. ***A***, ***B***, Retinal vibratome sections from P21 WT (***A***) and $Crx^{-/-}$ (***B***) mice labeled with antibodies against rhodopsin (magenta) and calbindin (green). ***C***, ***D***, Representative images of the OPL stained for CtBP2 in WT (***C***) and $Crx^{-/-}$ (***D***) retinas. ***E***, ***F***, Similar images of the OPL labeled with an antibody against VGluT1 in WT (***E***) and $Crx^{-/-}$ (***F***) background. ***G***, ***H***, Fluorescently conjugated PNA was used to mark active zones of cone spherules in WT (***G***) and $Crx^{-/-}$ (***H***) mice. ***I***, ***J***, OPL stained for the Ca^{2+} channel subunit CACNA1S, which normally localizes to dendritic tips of ON BCs (Claes et al., 2004), in WT (***I***) and $Crx^{-/-}$ (***J***) retinas.

Results

In $Crx^{-/-}$ mice, photoreceptors (PRs) fail to extend outer segments, the cellular compartment in which phototransduction occurs, and as a result do not respond to light (Furukawa et al., 1999). In addition, ultrastructural examination of rod and cone PRs in $Crx^{-/-}$ mice revealed severely abnormal synaptic terminals in the outer plexiform layer (OPL) (Morrow et al., 2005). Similar defects were observed in PRs expressing a dominant-negative form of Crx (Furukawa et al., 1997).

Contacts in the outer retina of $Crx^{-/-}$ mice lack proteins associated with presynaptic and postsynaptic specialization

We began our analysis of $Crx^{-/-}$ mice by testing whether the previously described ultrastructural abnormalities of PRs are accompanied by alterations in the expression and localization of proteins involved in phototransduction and synaptic trans-

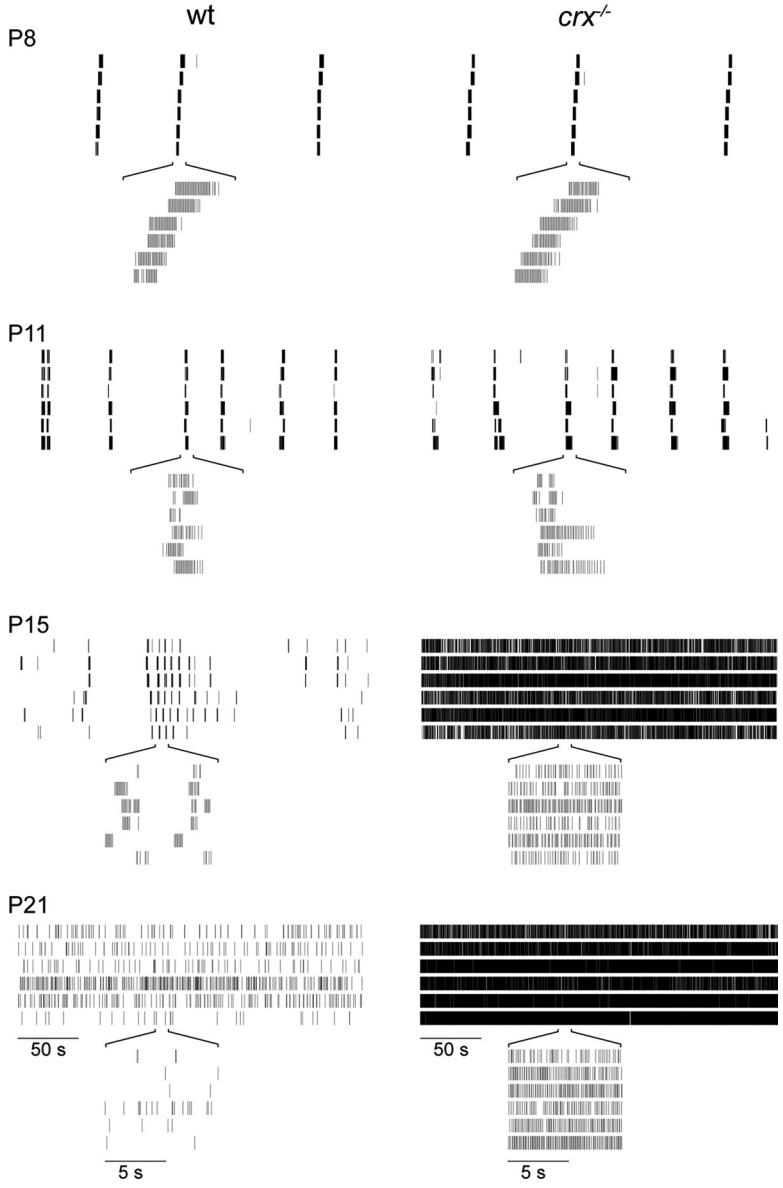

Figure 2. Spontaneous activity patterns in WT and $Crx^{-/-}$ retinas diverge with maturation. Raster plots illustrate (on 2 timescales) the firing patterns of six simultaneously recorded representative RGCs in WT (left column) and $Crx^{-/-}$ mice (right column). Activity was monitored at different developmental stages: P8 (cholinergic waves), P11 (glutamatergic waves), P15 (eye opening), and P21 (retinal circuits mostly mature). Whereas wave patterns are similar between WT and $Crx^{-/-}$ mice, activity begins to diverge drastically around the time of eye opening. Thus, firing in $Crx^{-/-}$ RGCs increases in frequency compared with WT and appears become rhythmic (see finer timescales) starting at ~P15.

mission. Immunohistochemistry on retinal vibratome sections [postnatal day 21 (P21)] showed that rhodopsin (the photopigment of rod PRs), which normally localizes to outer segments (Fig. 1*A*), is redistributed throughout rod PRs when their outer segments fail to develop (Fig. 1*B*). In addition, staining for calbindin, which labels horizontal cells, revealed a disorganized OPL in $Crx^{-/-}$ mice (Fig. 1*A*,*B*). We analyzed the expression of proteins involved in transmitter release from PR terminals by staining for CtBP2 (a component of presynaptic ribbons; Fig. 1*C*,*D*) and VGluT1 (the vesicular glutamate transporter used by PRs; Fig. 1*E*,*F*). Both of these proteins appear less abundant and mislocalized in $Crx^{-/-}$ mice. Moreover, labeling with fluorescent peanut agglutinin (PNA), which selectively marks cone active zones in WT mice (Fig. 1*G*) (Wässle et al., 2009), was absent in $Crx^{-/-}$ retinas (Fig. 1*H*). We next examined the molecular differentiation of the postsynapse on BC dendrites by labeling sections with antibodies against the L-type Ca^{2+} channel α-subunit CACNA1S (Fig. 1*I*,*J*) (Claes et al., 2004). The number and regularity of clusters formed by these channels on BC dendrites was greatly reduced in $Crx^{-/-}$ compared with WT mice. Together, these experiments show that key proteins involved in signal transmission are absent or mislocalized in the OPL of $Crx^{-/-}$ mice and, in conjunction with a previous ultrastructural study (Morrow et al., 2005), indicate that PRs fail to develop normal synaptic connections with BCs in these retinas.

Around the time of eye opening, RGCs become rhythmically hyperactive in $Crx^{-/-}$ mice

To test how abnormal synaptic development in the outer retina affects spontaneous activity in the inner retina, we recorded RGC spike trains on multielectrode arrays at different stages of development. We first confirmed that no short-latency light responses could be elicited from RGCs in $Crx^{-/-}$ mice (P21) over a broad range of stimulus intensities (0.01–50,000 Rh*/R/s; data not shown) (Furukawa et al., 1999). Before eye opening, circuits in the inner retina generate spontaneous activity in periodic bursts that spread among neighboring RGCs (Wong, 1999; Blankenship and Feller, 2010). Distinct circuit mechanisms initiate and propagate these retinal waves during different periods of development (Wong, 1999; Blankenship and Feller, 2010). Figure 2 illustrates the associated changes in the spatiotemporal patterns of retinal waves in WT and $Crx^{-/-}$ mice. At P8, a network of cholinergic amacrine cells (ACs) mediates retinal waves with long refractory periods and bursts lasting ~2 s (Feller et al., 1996; Demas et al., 2003; Zheng et al., 2006). By P11, glutamate release from BCs drives wave activity, resulting in shorter bursts of activity and shorter silent intervals between them (Demas et al., 2003; Kerschensteiner and Wong, 2008; Blankenship et al., 2009). Activity patterns during cholinergic and glutamatergic waves were indistinguishable between $Crx^{-/-}$ and WT mice. At approximately P15, mice open their eyes and retinal waves decline as visually evoked activity begins to dominate the retina (Demas et al., 2003; Kerschensteiner and Wong, 2008). At this age, the spontaneous activity patterns of RGCs in WT and $Crx^{-/-}$ mice diverged. To quantify changes in activity, we calculated the average rate and power spectrum of each RGC spike train and analyzed correlation indices of cell pairs as a function of the distance separating the electrodes on which they were recorded. As illustrated by the representative spike rasters (Fig. 2), the average firing rates (Fig. 3*A*) of RGCs in $Crx^{-/-}$ mice increased sharply compared with WT littermates at P15 (WT, 0.66 ± 0.07 Hz, $n = 231$ cells; $Crx^{-/-}$, 2.51 ± 0.21 Hz, $n = 163$ cells; $p < 10^{-30}$, mean ± SEM) and remained elevated at

P21 (WT, 1.65 ± 0.13 Hz, $n = 197$ cells; $Crx^{-/-}$, 5.15 ± 0.37 Hz, $n = 224$ cells; $p < 10^{-12}$). In addition, the activity of RGCs in $Crx^{-/-}$ mice became oscillatory, evidenced by large peaks in the power spectra at fundamental frequencies of ~2.4 and ~5 Hz in P15 and P21 retinas, respectively (Fig. 3*B*), and smaller peaks at the harmonics. Finally, because activity during waves propagates across the surface of the retina, correlation indices (see Materials and Methods) fall off smoothly with increasing distance between RGCs at P8 (data not shown) and P11 in both WT and $Crx^{-/-}$ mice (Fig. 3*C*). In comparison, correlation indices for both genotypes were low after P15, indicating that the oscillatory activity in $Crx^{-/-}$ retinas did not propagate in a wave-like manner.

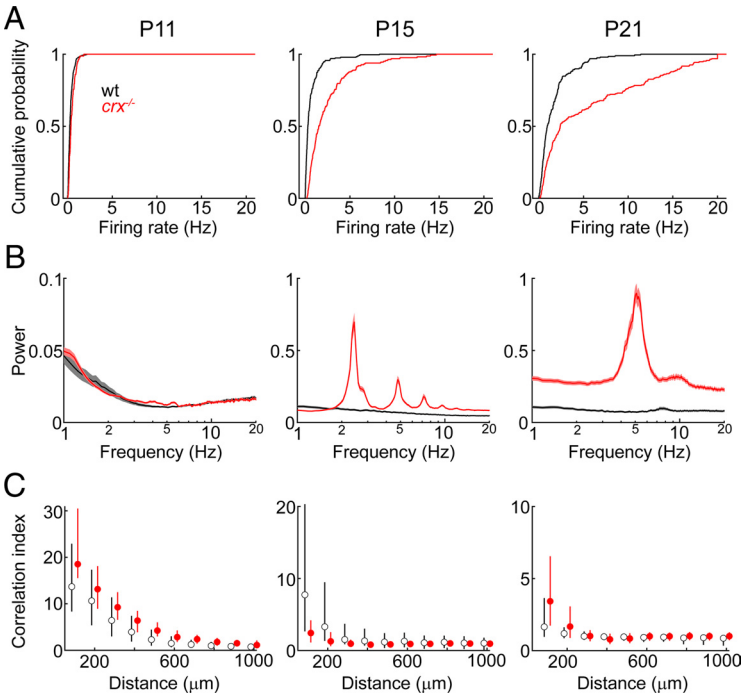

Figure 3. RGCs develop oscillatory hyperactivity in $Crx^{-/-}$ mice. ***A***, Cumulative distributions of average firing rates of RGCs in WT (black lines) and $Crx^{-/-}$ (red lines) mice recorded at P11 (left column; WT, $n = 253$ cells; $Crx^{-/-}$, $n = 78$ cells), P15 (middle column; WT, $n = 231$ cells; $Crx^{-/-}$, $n = 163$ cells), and P21 (right column; WT, $n = 197$ cells; $Crx^{-/-}$, $n = 224$ cells). ***B***, Power spectra of RGC spike trains at the different ages normalized to the peak power of the P21 $Crx^{-/-}$ dataset. Lines (shaded areas) represent mean ± SEM of the population. Black indicates data from WT and red from $Crx^{-/-}$ mice. ***C***, Correlation indices of RGC activity at different ages plotted as a function of the distance separating the electrodes on which the respective spike trains were recorded. Circles (WT, black; $Crx^{-/-}$, red) indicate median of the population and lower and upper ends of the error bars the 25th and 75th percentile, respectively.

Neurotransmitter release from BCs is increased in $Crx^{-/-}$ mice

The increased spontaneous spiking of RGCs beginning at approximately P15 could be caused by either increased excitatory input from BCs or changes in the intrinsic excitability of RGCs. In *rd1* mice, in which RGCs become hyperactive as PRs degenerate, the underlying changes were found to be presynaptic to RGCs (Margolis et al., 2008; Borowska et al., 2011). We therefore recorded spontaneous EPSCs (sEPSCs) from large monostratified RGCs in $Crx^{-/-}$ and WT mice at P15. We targeted RGCs with large somata (~20 μm) and identified cell types based on their dendritic morphology revealed by two-photon imaging at the end of the recording (Fig. 4*A*,*B*). Results for ON and OFF RGCs were indistinguishable and were therefore combined. Representative sEPSC traces (Fig. 4*C*) and a comparison of their power spectra (Fig. 4*D*) illustrate that neurotransmitter release from BCs in $Crx^{-/-}$ but not WT mice oscillated with a fundamental frequency (~3.3 Hz) similar to that observed in the spike trains of RGCs at this age (~2.5 Hz). In addition, the input level quantified by the charge transfer through EPSCs was increased 2.5 ± 0.5-fold (WT, $n = 6$ cells; $Crx^{-/-}$, $n = 13$ cells; $p < 0.03$) in $Crx^{-/-}$ compared with WT retinas (Fig. 4*E*). Thus, in the absence of normal PR input, BCs become hyperactive and drive RGCs to oscillatory spontaneous bursting.

Laminar organization of BC, AC, and RGC neurites in the inner plexiform layer of $Crx^{-/-}$ mice is preserved

In the inner retina, functionally distinct connections are confined to separate sublaminae of the inner plexiform layer (IPL) (Wässle, 2004). To test the influence of spontaneous activity and PR input on the laminar organization of the inner retina, we compared the distribution of cell-type-specific markers in the IPL of WT and $Crx^{-/-}$ mice at P21. Axons of RB (Fig. 5*A*,*B*, PKCα) as well as type 2 (B2) and B6 cone BCs (B2 brightly labeled with anti-SytII, B6 dimly labeled with anti-SytII; Fig. 5*C*,*D*) targeted correct IPL sublaminae in the absence of functional PRs. Likewise, neurites of different AC populations labeled with antibodies against calretinin (Fig. 5*E*,*F*), VGluT3 (Fig. 5*G*,*H*), and ChAT (Fig. 5*I*,*J*) showed normal lamination patterns in $Crx^{-/-}$ mice. To study the stratification of dendrites of an identified RGC type, we crossed BAC transgenic mice (*DRD4–EGFP*), which express EGFP in DSGCs responding preferentially to motion in the posterior direction, to $Crx^{-/-}$ mice (Huberman et al., 2009). Stratification patters of these DSGCs were unchanged in $Crx^{-/-}$ compared with WT background. Thus, for the BC, AC, and RGC types tested here, normal spontaneous or evoked activity patterns from P15 onward appear not required for appropriate laminar organization in the IPL.

Mosaics of cholinergic ACs and DSGCs develop normally in $Crx^{-/-}$ mice

In addition to the vertical organization of neurites into layers, the cell bodies of retinal neurons show regular horizontal distributions. Their arrangement into mosaics is thought to help neuronal cell types cover the retinal surface evenly and represent visual space homogeneously (Masland, 2001; Wässle, 2004). To what extent activity regulates the formation and maintenance of mosaics is incompletely understood (Zhang et al., 2005; Lee et al., 2007; Anishchenko et al., 2010). We analyzed the lateral distribution of two representative cell types in the inner retina. The density of posterior motion-selective DSGCs (Fig. 6*A*,*B*; WT, 214 ± 14 cells/mm^2, $n = 17$ retinas; $Crx^{-/-}$, 225 ± 20 cells/mm^2, $n = 9$ retinas, mean ± SEM; $p > 0.9$) and the regularity of their distribution measured by the average distance between nearest neighbors of the same cell type (Fig. 6*C*; WT, 39.2 ± 1.9 μm; $Crx^{-/-}$, 37.5 ± 1.4 μm, mean ± SEM; $p > 0.8$) and the effective radius of density recovery profiles (Rodieck, 1991) (Fig. 6*D*; WT, 25.5 ± 1.9 μm; $Crx^{-/-}$, 25.5 ± 2.5 μm, mean ± SEM; $p > 0.9$) were unchanged

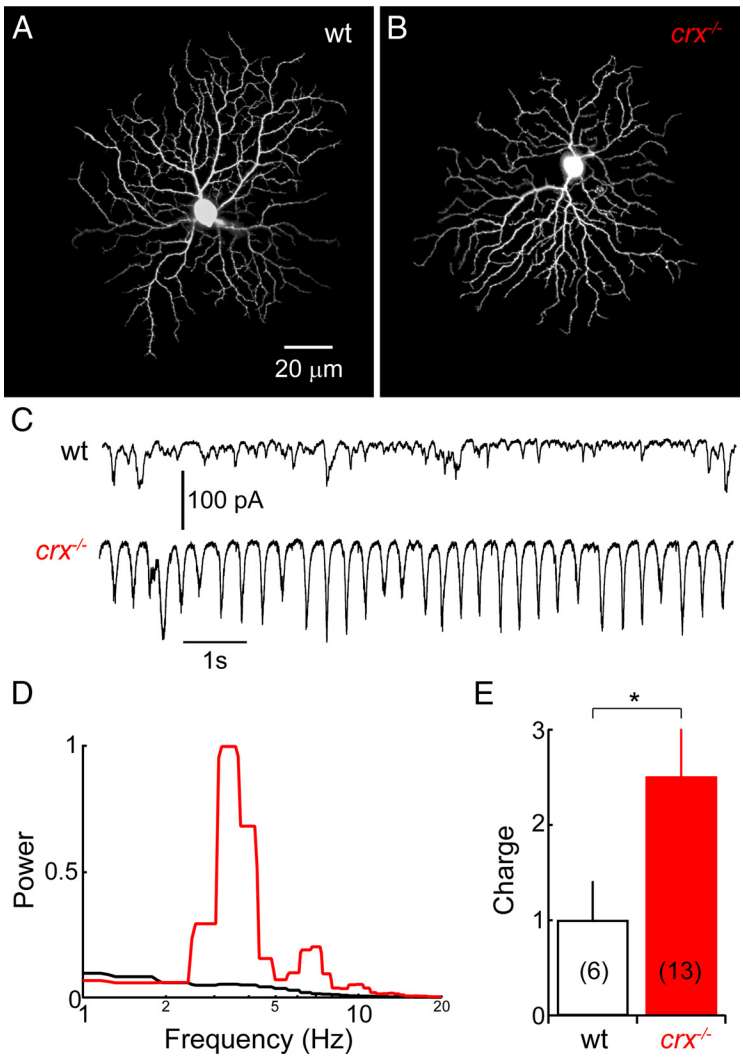

Figure 4. RGCs in $Crx^{-/-}$ mice receive increased spontaneous synaptic input from BCs. ***A***, ***B***, Representative *z*-projections of two-photon image stacks of RGCs filled with Alexa Fluor 568, acquired after whole-cell recordings in P15 WT (***A***) and $Crx^{-/-}$ (***B***) retinas. ***C***, ***D***, Traces of sEPSCs recorded from the cells shown in ***A*** and ***B***, respectively, reveal elevated and oscillatory synaptic input to RGCs in $Crx^{-/-}$ (bottom trace) compared with WT (top trace) mice. ***E***, Power spectra (normalized to maximum power across traces) of sEPSCs show a large peak at a fundamental frequency of ~3.3 Hz in $Crx^{-/-}$ (red line) but not in WT (black line) mice. ***F***, Charge transfer associated with sEPSCs (normalized to average of the WT dataset). Bars and error bars indicate mean ± SEM of the population. The number of cells included in the analysis is shown in parentheses. $^*p < 0.05$.

in $Crx^{-/-}$ compared with WT mice. Similarly, the density (Fig. 6*E*,*F*; WT, 1070 ± 80 cells/mm^2, $n = 16$ retinas; $Crx^{-/-}$, 950 ± 41 cells/mm^2, $n = 15$ retinas, mean ± SEM; $p > 0.3$), nearest-neighbor distances (Fig. 6*G*; WT, 20.2 ± 0.6 μm; $Crx^{-/-}$, 20.1 ± 0.3 μm, mean ± SEM; $p > 0.1$), and effective radii (Fig. 6*H*; WT, 15.7 ± 0.6 μm; $Crx^{-/-}$, 16.4 ± 0.4 μm, mean ± SEM; $p > 0.06$) of cholinergic ACs in the ganglion cell layer were not significantly different between both genotypes. Qualitatively similar results were obtained for cholinergic ACs in the inner nuclear layer (data not shown). These observations suggest that the mosaic organization of representative neuron types in the retina is primarily independent of spontaneous activity or light-evoked signaling.

Synaptogenesis on RGC dendrites with normal branching patterns is enhanced in $Crx^{-/-}$ mice

We have shown previously that, when glutamate release from BCs is reduced, their axons form fewer synapses with RGC dendrites (Kerschensteiner et al., 2009). To test whether activity promotes synaptogenesis rather than being merely required for its normal occurrence, we biolistically (i.e., using a gene gun) labeled RGCs in WT (Fig. 7*A–C*) and $Crx^{-/-}$ (Fig. 7*D–F*) retinas with tdTomato (a red cytosolic fluorophore) and PSD95–YFP (a marker of excitatory synapses on RGC dendrites) at P9 (Fig. 7*A*,*D*), P15 (Fig. 7*B*,*E*), and P25 (Fig. 7*C*,*F*) (Jakobs et al., 2008; Morgan et al., 2008). Using custom-written image analysis software (Morgan et al., 2008; Kerschensteiner et al., 2009), we reconstructed the branching patterns of dendritic trees and mapped the distribution of excitatory synapses on them. To avoid mistaking differences between cell types for developmental changes or phenotypes of $Crx^{-/-}$ mice, we restricted our analysis to large monostratified RGCs within the ON sublamina of the IPL. However, results were qualitatively similar when all cell types were included (data not shown). Across development from P9 to P25, dendritic branching of these RGCs became sparser (Fig. 7*G*, $p < 0.001$, ANOVA), absolute stratification width grew slightly (Fig. 7*H*, $p < 0.05$, ANOVA), and the density of synapses on them increased from P9 to P16 (Fig. 7*I*, $p < 10^{-5}$, ANOVA) in agreement with previous findings (Coombs et al., 2007; Morgan et al., 2008; Soto et al., 2011). Neither lateral branching nor laminar targeting differed significantly between RGCs in $Crx^{-/-}$ and WT mice ($p > 0.1$). However, after the onset of hyperactivity, the density of excitatory synapses on RGCs increased in $Crx^{-/-}$ compared with WT mice (P16; WT, 0.36 ± 0.04 synapses/μm, $n = 9$ cells; $Crx^{-/-}$, 0.41 ± 0.03 μm, $n = 8$ cells, mean ± SEM; $p > 0.4$), with the difference reaching significance at P25 (WT, 0.35 ± 0.03 synapses/μm, $n = 12$ cells; $Crx^{-/-}$, 0.46 ± 0.04 μm, $n = 11$ cells, mean ± SEM; $p < 0.03$).

Elevated spontaneous activity selectively increases the rate of synapse formation in $Crx^{-/-}$ mice

During development, synapses between BCs and RGCs turn over relatively rapidly (Kerschensteiner et al., 2009). Therefore, the increase in synapse numbers observed in $Crx^{-/-}$ compared with WT mice could be the result of more frequent synapse formations, fewer synapse eliminations, or a combination of both. To distinguish between these possibilities, we performed live-imaging experiments in which we tracked the appearance and disappearance of PSD95–YFP clusters on dendrites of large monostratified ON RGCs in a time-lapse series (Fig. 8*A–C*). We have shown previously that newly formed PSD95–YFP clusters are apposed by presynaptic ribbons and colocalize with postsynaptic glutamate receptors, whereas axo-dendritic appositions without PSD95–YFP clusters are and do neither (Kerschensteiner et al., 2009; Morgan et al., 2011). Thus, appearances and disap-

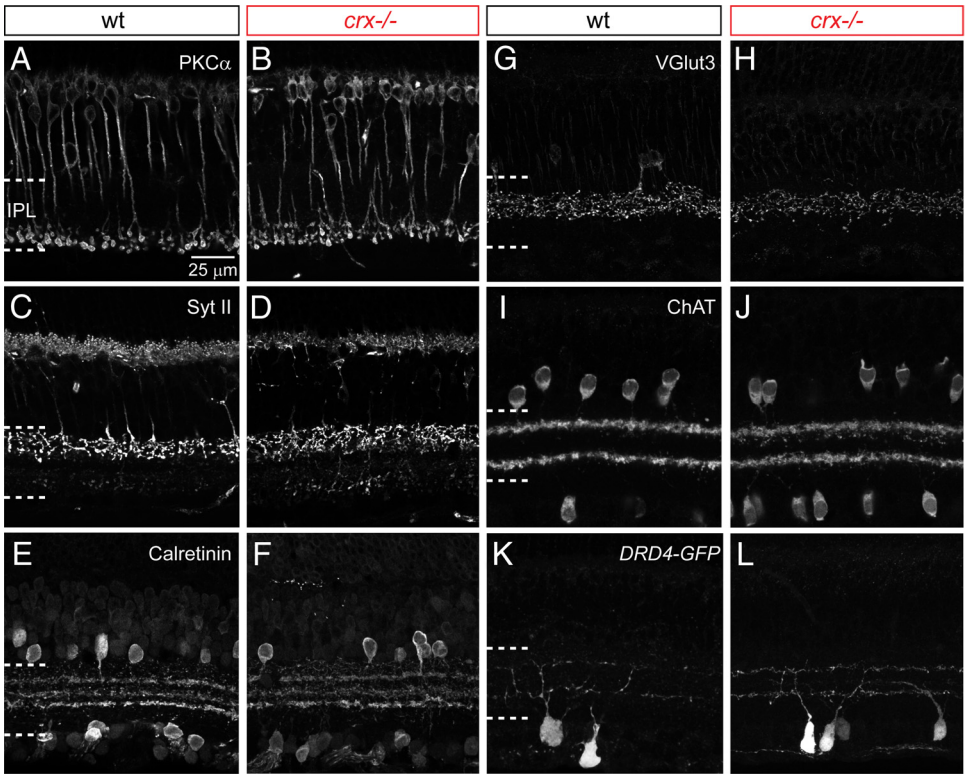

Figure 5. Normal laminar targeting of BCs, ACs, and RGCs in the IPL of $Crx^{-/-}$ mice. ***A***, ***B***, RB cells in retinal vibratome sections from P21 WT (***A***) and $Crx^{-/-}$ (***B***) mice labeled by immunohistochemistry (PKCα). ***C***, ***D***, In the IPL (dashed lines) of WT (***C***) and $Crx^{-/-}$ (***D***) retinas, staining for SytII brightly labels axon terminals of B2 BCs and dimly labels axon terminals of B6 BCs. ***E***, ***F***, AC processes visualized with an antibody against calretinin form three distinct bands in the IPL of WT (***E***) and $Crx^{-/-}$ (***F***) mice. ***G***, ***H***, A single type of AC stratifying toward the center of the IPL expresses VGluT3 in WT (***G***) and $Crx^{-/-}$ (***H***) retinas. ***I***, ***J***, Cholinergic ACs (expressing ChAT) are found in the ganglion cell layer and inner nuclear layer stratifying their processes in the inner and outer half of the IPL, respectively, of WT (***I***) and $Crx^{-/-}$ (***J***) mice. ***K***, ***L***, Posterior motion-selective DSGCs are labeled by transgenic expression of GFP (amplified by immunohistochemistry) in *DRD4–EGFP* mice (Huberman et al., 2009) in WT (***K***) and $Crx^{-/-}$ (***L***) backgrounds.

pearances of PSD95–YFP clusters in this system reliably indicate synapse formation and elimination events, respectively. We measured the rates of PSD95–YFP cluster formation and elimination at P16, when spontaneous glutamate release from BCs is increased (Fig. 4), and connectivity patterns between BC and RGCs begin to diverge between $Crx^{-/-}$ and WT mice (Fig. 7). We found that, compared with WT mice, the rate of synapse formation was increased several-fold in $Crx^{-/-}$ retinas (Fig. 8*D*; WT, 21 ± 4 synapses/mm dendrite/24 h, $n = 14$ cells; $Crx^{-/-}$, 85 ± 9 synapses/mm dendrite/24 h, $n = 13$ cells, mean ± SEM; $p < 10^{-4}$), whereas synapse elimination was unchanged (Fig. 8*E*; WT, 6.8 ± 1.2% of synapses/24 h; $Crx^{-/-}$, 7.1 ± 0.8% of synapses/24 h, mean ± SEM; $p > 0.8$).

The effects of increased spontaneous activity are cell-type dependent among converging BCs in $Crx^{-/-}$ mice

To better understand how spontaneous activity regulates synaptogenesis in the context of an intact circuit, we wanted to determine whether its effects are uniform or distinct among different BC types converging onto a shared RGC target. These experiments require simultaneous and spectrally separable labeling of isolated presynaptic and postsynaptic neurons and their connections in the intact retina. To achieve this, we made use of transgenic mice in which three types of BCs (B6, B7, and RB) express tdTomato (*Grm6–tdTomato*). In *Grm6–tdTomato* mice, few cells fluoresce brightly and can thus be reconstructed in isolation (Kerschensteiner et al., 2009). We crossed *Grm6–tdTomato* mice to $Crx^{-/-}$ mice and biolistically labeled RGCs with cytosolic CFP and PSD95–YFP. We restrict our analysis to G10 RGCs because axons of B6, B7, and RB cells converge onto their dendrites. In addition, G10 RGCs are easily identified based on their characteristic morphology (Völgyi et al., 2009; Morgan et al., 2011). We counted synapses in BC–RGC pairs through plane-by-plane inspection of confocal imaging stacks (Fig. 9*A–F*). A synapse was assigned to a pair when a PSD95–YFP punctum coincided with a region where axonal and dendritic fluorescence overlapped. In this way, we analyzed the connectivity of 109 BC–RGC pairs in P21 retinas. Strikingly, B6 cells more than doubled the number of synapses with G10 dendrites in $Crx^{-/-}$ compared with WT backgrounds (Fig. 9*A*,*D*,*G*; WT, 4.2 ± 0.5 synapses/pair, $n = 25$ pairs; $Crx^{-/-}$, 8.9 ± 0.9 synapses/pair, $n = 23$ pairs, mean ± SEM; $p < 10^{-4}$). In contrast, connectivity patterns from B7 to G10 cells were indistinguishable between the two genotypes (Fig. 9*B*,*E*,*G*, inset; WT, 2.4 ± 0.5 synapses/pair, $n = 8$ pairs; $Crx^{-/-}$, 2.3 ± 0.6 synapses/pair, $n = 12$ pairs, mean ± SEM; $p > 0.7$) and RB axons while frequently being apposed to G10 dendrites (Fig. 9*C*,*F*,*G*; WT, 1.2 ± 0.1 appositions/pair, $n = 16$ pairs; $Crx^{-/-}$, 1.3 ± 0.1 appositions/pair, $n = 24$ pairs, mean ± SEM; $p > 0.6$) with which they form synapses earlier in development (Morgan et al., 2011) lose their connections in both $Crx^{-/-}$ and WT retinas (Fig. 9*C*,*F*,*G*; WT, 0.06 ± 0.06 synapses/pair; $Crx^{-/-}$, 0.13 ± 0.07 synapses/pair, mean ± SEM; $p > 0.5$). We recently found that axonal boutons of B6 cells can form multisynaptic appositions with G10 dendrites (Morgan et al., 2011). In multisynaptic appositions, several matched presynaptic and postsynaptic specializations are contained within continuous areas of axo-dendritic overlap. In $Crx^{-/-}$ mice, the frequency of these multisynaptic appositions is increased and shifted toward connections of higher

order (Fig. 9*H*; WT, 0.95 ± 0.08 synapses/apposition, $n = 25$ pairs; $Crx^{-/-}$, 1.87 ± 0.13 synapses/apposition, $n = 23$ pairs, mean ± SEM; $p < 10^{-6}$).

Hyperactive RGCs maintain normal axonal projection patterns in dLGN

Spontaneous activity patterns of RGCs have been shown to shape their axonal projections (Huberman et al., 2008a). Thus, both the development and maintenance of segregation of axons from the ipsilateral and contralateral eye in the dLGN are thought to depend on normal activity (Dubin et al., 1986; Penn et al., 1998; Chapman, 2000; Pfeiffenberger et al., 2005; Torborg et al., 2005; Demas et al., 2006). To test whether eye-specific segregation in dLGN was disrupted by the oscillatory hyperactivity of RGCs in $Crx^{-/-}$ mice, we injected, at P21, β-cholera toxins conjugated to Alexa Fluor 488 and Alexa Fluor 594, respectively, into opposite eyes and assessed the distribution of fluorescence in the dGLN 1–2 d later. Quantified by the variance of the $\log_{10}$ ratios of the two fluorescence signals (see Materials and Methods) (Torborg and Feller, 2004), eye-specific segregation of RGC axons in dLGN was indistinguishable between WT and $Crx^{-/-}$ mice (Fig. 10*A–F,K*; WT, 0.46 ± 0.13, $n = 6$ dLGNs; $Crx^{-/-}$, 0.46 ± 0.04, $n = 8$ dLGNs, mean variance ± SEM; $p > 0.9$).

In addition to eye-specific segregation, axons of different RGC types have been shown recently to occupy distinct layers in the mouse dLGN (Huberman et al., 2008b, 2009; Kim et al., 2010). To what extent the maintenance of these lamination patterns that emerge before P10 depend on activity remained unknown. We therefore crossed *DRD4–EGFP* mice to $Crx^{-/-}$ mice. Our results showed that, as in WT mice, the axons of this RGC type occupy a tight band in the lateral portion of the dLGN in $Crx^{-/-}$ mice (Fig. 10*G–J,L*).

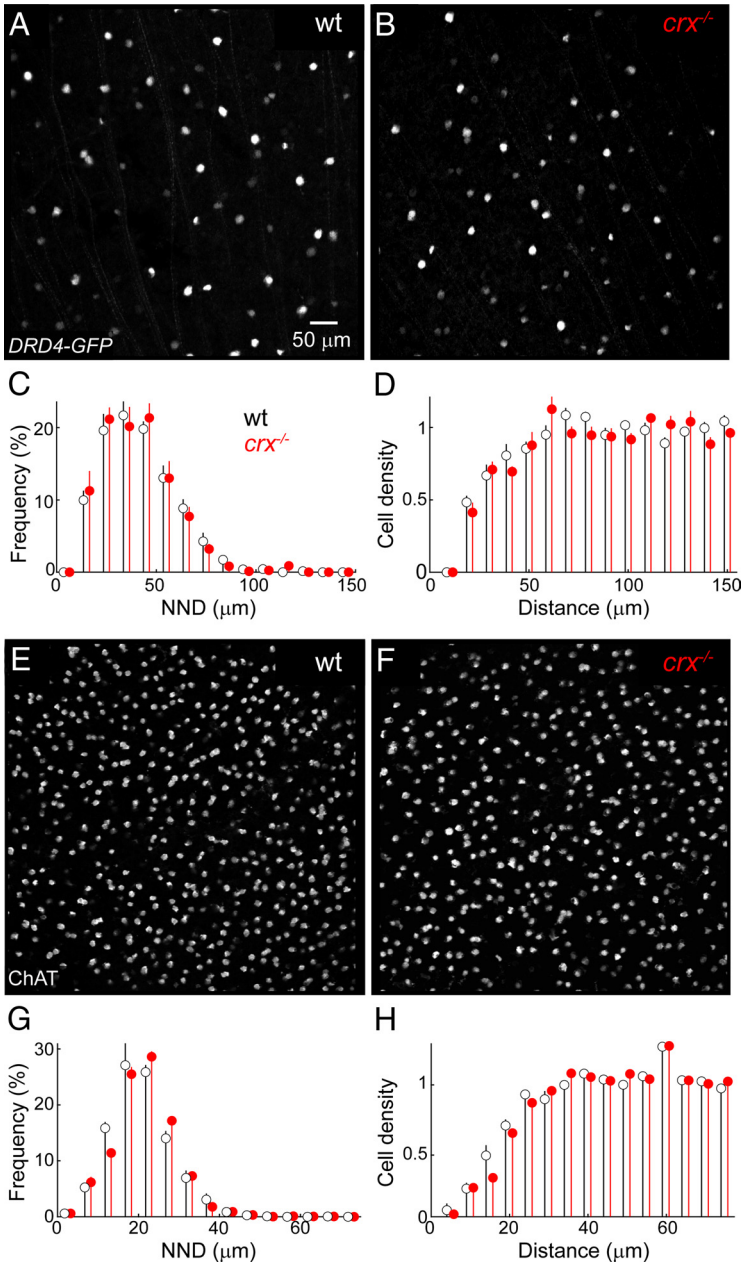

Figure 6. Mosaics of cholinergic ACs and DSGCs are preserved in $Crx^{-/-}$ mice. ***A***, ***B***, Maximum intensity projections of representative confocal image stacks of posterior motion-selective DSGCs expressing GFP (*DRD4–EGFP*) acquired from flat-mount preparations of WT (***A***) and $Crx^{-/-}$ (***B***) retinas. ***C***, Distributions of nearest-neighbor distances (NND) between GFP-expressing DSGCs in WT (black open circles) and $Crx^{-/-}$ (red filled circles) background. Circles (overshoot) represent mean ± SEM of the population data (WT, $n = 17$ retinas; $Crx^{-/-}$, $n = 9$ retinas). ***D***, Density recovery profiles for GFP-expressing DSGCs. For randomly distributed cells, histograms are expected to be flat around the average density (normalized to 1). A dip in the density of cells of the same type close to the origin indicates the existence of an exclusion zone characteristic of mosaic distributions. Color coding and symbols analogous to ***C***. ***E***, ***F***, Representative maximum intensity projections (same magnification as ***A***) through confocal image stacks of cholinergic ACs (stained for ChAT) in the ganglion cell layer. ***G***, ***H***, Analogous to ***C*** and ***D*** for ChAT-positive rather than GFP-expressing cells. Population data are based on 16 and 15 retinas from WT and $Crx^{-/-}$ mice, respectively.

Despite additional hyperactivity, BC–RGC synapse numbers and eye-specific segregation of RGC axons in dLGN remain stable in older $Crx^{-/-}$ mice

During development, many neural circuits are particularly receptive to activity-dependent synaptic refinement during critical periods (Hensch, 2004). The existence and timing of such a phase of heightened synaptic plasticity in the retina remain unknown. We first wanted to test whether hyperactivity persists in older $Crx^{-/-}$ mice and, if so, analyze its effects on BC–RGC connectivity. Recordings of spike trains from ensembles of RGCs in 4- to 6-month-old $Crx^{-/-}$ mice and WT littermates showed that, in fact, spontaneous activity was further elevated at this age (Fig. 11*A,B*; WT, 2.31 ± 0.35 Hz, $n = 201$ cells; $Crx^{-/-}$, 12.66 ± 0.77 Hz, $n = 167$ cells, mean ± SEM; $p < 10^{-39}$). Accordingly, RGC spiking in $Crx^{-/-}$ mice was oscillatory with a higher fundamental frequency than at younger ages (Fig. 11*C*, ~8.6 Hz). Despite this additional increase in spontaneous activity, however, the densities of BC synapses on RGC dendrites in 6-month-old $Crx^{-/-}$ and WT mice were indistinguishable from those observed at P25 ($p > 0.3$) and remained stably elevated for $Crx^{-/-}$ compared with WT RGCs

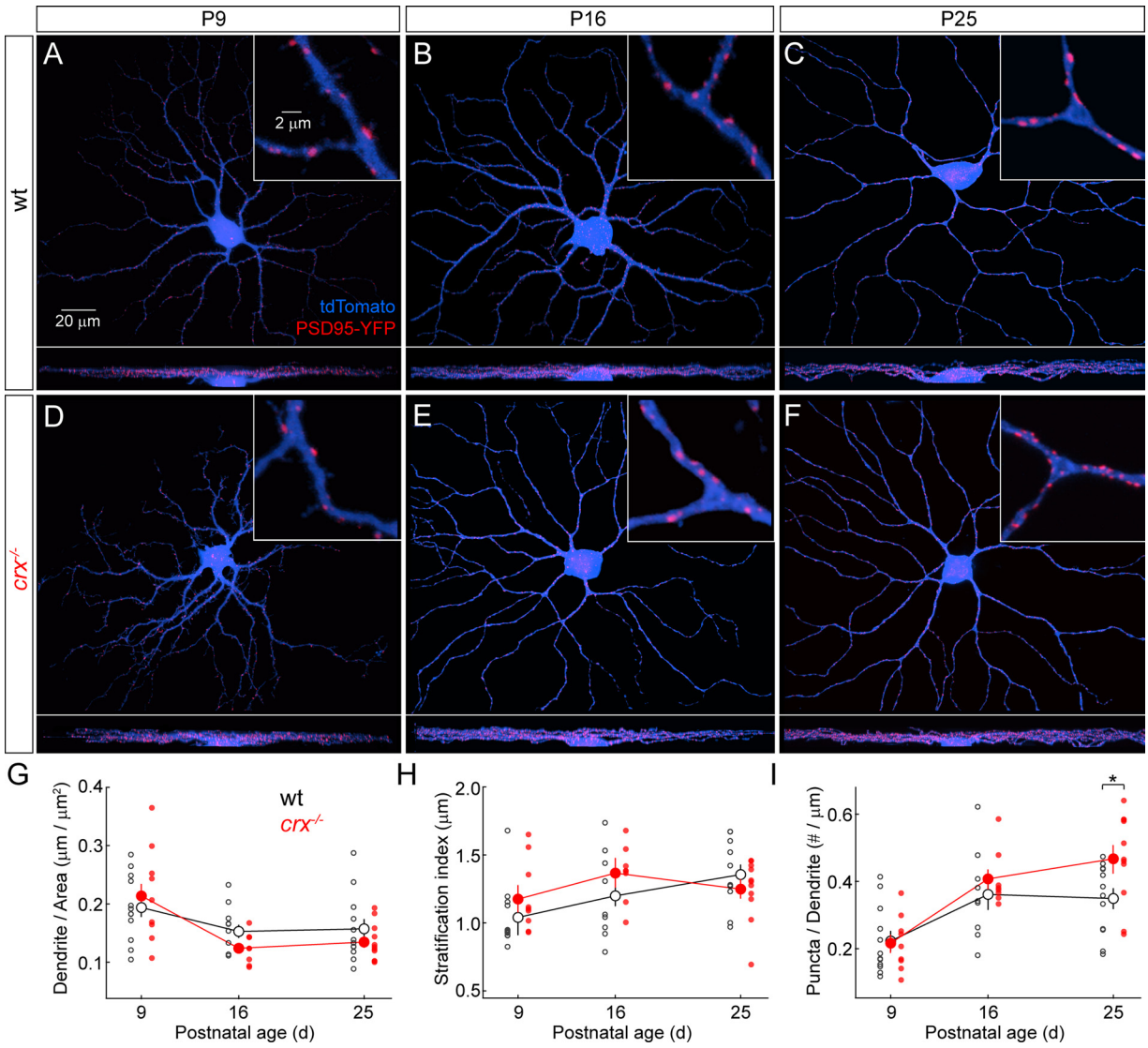

Figure 7. Density of excitatory synapses on RGC dendrites increases after onset of hyperactivity in $Crx^{-/-}$ compared with WT mice. ***A–F***, Representative maximum intensity *z*-projections (top panels) and *y*-projections (bottom panels) of confocal image stacks from RGCs biolistically labeled with tdTomato (blue) and PSD95–YFP (red) in WT (***A–C***) and $Crx^{-/-}$ (***D–F***) mice at P9 (***A***, ***D***), P16 (***B***, ***E***), and P25 (***C***, ***F***). Insets show higher-magnification views of excerpts from the *z*-projections. ***G***, Dendritic density (dendrite length/area) of RGCs biolistically labeled in WT (black) and $Crx^{-/-}$ (red) background plotted as a function of postnatal age. Throughout the figure, small circles represent average values of one cell and are offset for visual clarity. Large circles and error bars indicate the mean ± SEM across all cells of a given genotype. ***H***, Width of RGC dendritic stratification plotted across development. ***I***, Density of excitatory synapses onto RGC dendrites diverges between WT and $Crx^{-/-}$ retinas at approximately P16. *$p < 0.05$.

(Fig. 11*D*,*E*; WT, 0.32 ± 0.02 synapses/μm, $n = 4$ cells; $Crx^{-/-}$, 0.46 ± 0.04 μm, $n = 6$ cells, mean ± SEM; $p < 0.04$). We next analyzed whether the continued and more pronounced hyperactivity observed in older $Crx^{-/-}$ mice affected the eye-specific segregation of their RGC axons in the dLGN. Injections of β-cholera toxins conjugated to Alexa Fluor 488 and Alexa Fluor 594, however, revealed that the separation of axons from the ipsilateral and contralateral eyes was maintained in 4- to 6-month-old mice (Fig. 11*F*; WT, 0.58 ± 0.06, $n = 4$ dLGNs; $Crx^{-/-}$, 0.49 ± 0.03, $n = 4$ dLGNs, mean variance ± SEM; $p > 0.2$).

Discussion

In this study, we show that spontaneous activity promotes synaptogenesis and we analyze the dynamics, specificity, and critical period of this regulation in developing retinal circuits. Moreover, we determine the effects of spontaneous activity on laminar targeting and mosaic organization in the retina and the maintenance of retinogeniculate projection patterns.

Glutamate release from BCs promotes synaptogenesis with RGCs

Patch-clamp recordings revealed that the increased, rhythmic firing of RGCs in $Crx^{-/-}$ mice is generated at least in part by elevated excitatory input (Fig. 4). Similar increases in synaptic input to RGCs have been reported for *rd1* mice (Margolis et al., 2008; Stasheff, 2008). The mechanisms that cause circuits in inner retina to become hyperactive in the absence of normal input from the outer retina are incompletely understood but seem to involve electrical coupling of ACs and BCs (Borowska et al., 2011; Margolis and Detwiler, 2011).

Previous studies have demonstrated that, when spontaneous activity is suppressed, many developing circuits establish fewer

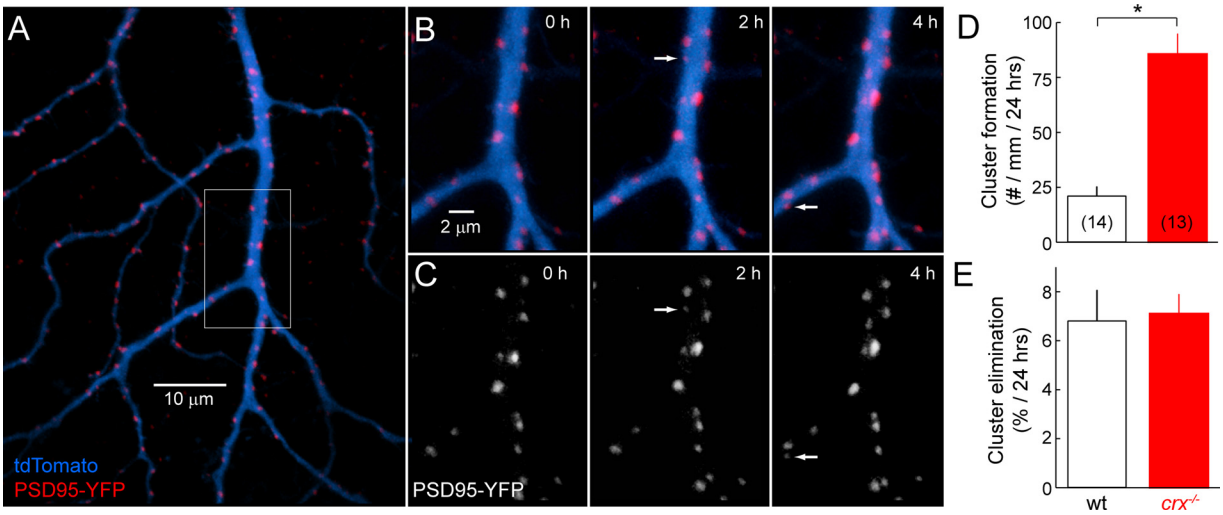

Figure 8. Elevated neurotransmission selectively increase the rate of synapse formation in $Crx^{-/-}$ mice. ***A***, First image of a time-lapse series of a large monostratified RGC in a P16 $Crx^{-/-}$ retina biolistically labeled with tdTomato (blue) and PSD95–YFP (red). ***B***, ***C***, Time series of the region indicated by the white box in ***A*** in which two new PSD95–YFP clusters form (arrows). The PSD95–YFP signal is shown in isolation in ***C***. ***D***, ***E***, Summary data (mean ± SEM) of the rates of PSD95–YFP cluster formation and elimination in WT and $Crx^{-/-}$ retinas (P16). In ***D***, the number of cells in each dataset is shown in parentheses. To avoid biases, cluster formation rates (***D***) were normalized to the length of dendrite imaged, and elimination rates (***E***) were expressed as the percentage of synapses lost. *$p < 0.05$.

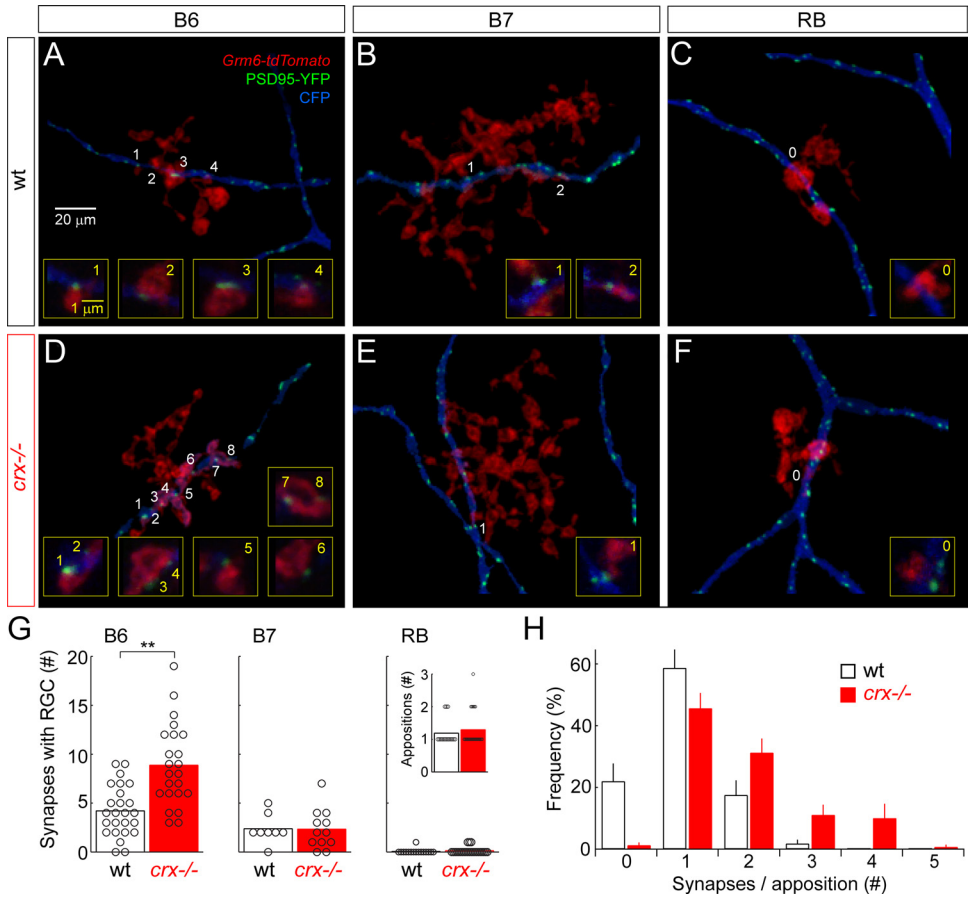

Figure 9. Synaptic development of converging BCs with a shared RGC target is altered in a cell-type-specific manner in $Crx^{-/-}$ mice. ***A–F***, Maximum intensity *z*-projections through confocal image stacks of BC–RGC pairs. Pairs consisted of B6 (***A***, ***D***), B7 (***B***, ***E***), or RB (***C***, ***F***) axons labeled by transgenic expression of tdTomato (*Grm6–tdTomato*; red) and G10 RGCs biolistically transfected with CFP (blue) and PSD95–YFP (green) in WT (***A–C***) and $Crx^{-/-}$ (***D–F***) background. Insets show synapses in higher-magnification views of single-image planes. In the *z*-projections (but not in the single-plane views), BCs were masked for visual clarity. ***G***, Population data for the number of synapses of B6–G10 (left), B7–G10 (middle), and RB–G10 (right) pairs. Each circle indicates the number of synapses for a single cell pair, and bars represent the mean of the respective populations in WT (white bar) and $Crx^{-/-}$ (red bar) mice. Inset in the right shows the number of appositions of RB–G10 pairs. **$p < 0.01$. ***H***, Histogram of synaptic constellations at appositions of B6–G10 pairs. Bars and error bars indicate mean ± SEM of WT (white bars) and $Crx^{-/-}$ (red bars) datasets.

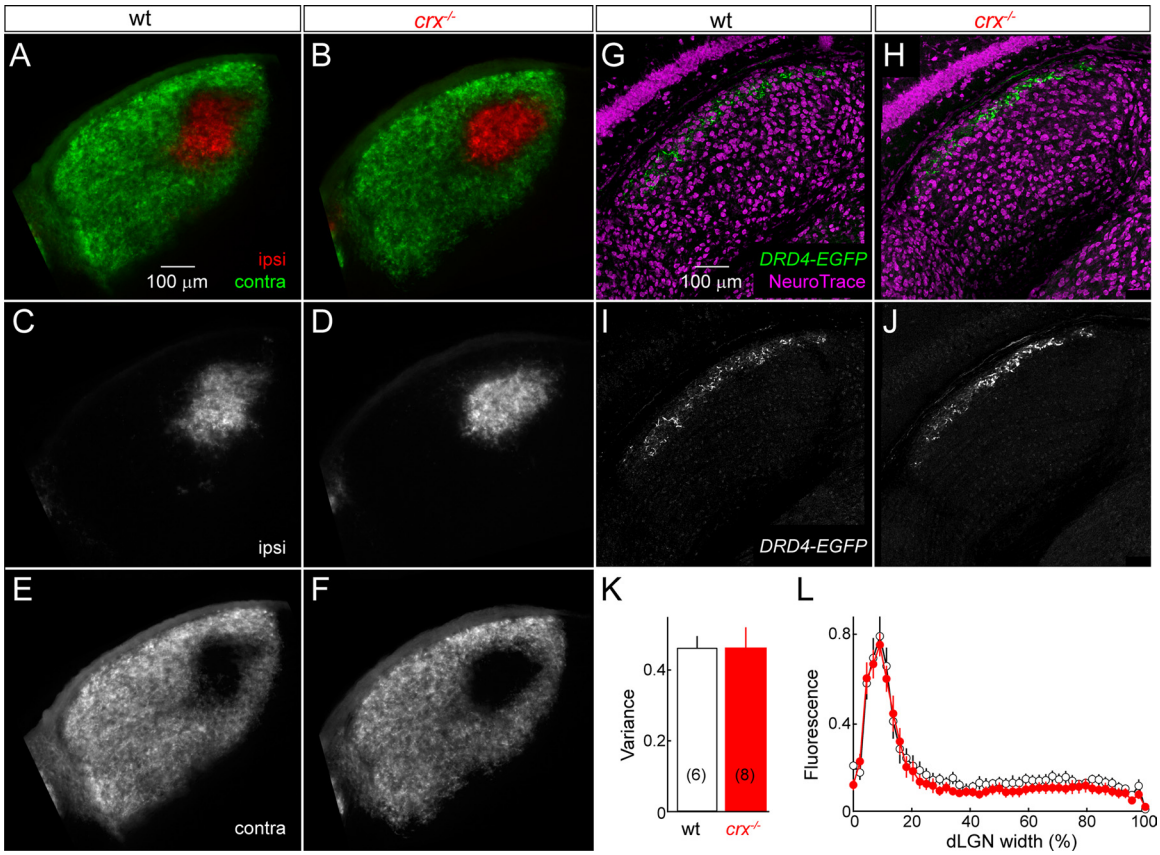

Figure 10. Hyperactive RGC axons maintain eye-specific segregation and laminar targeting in the dLGN of $Crx^{-/-}$ mice. ***A–F***, Coronal sections through dLGN of WT (***A***, ***C***, ***E***) and $Crx^{-/-}$ (***B***, ***D***, ***F***) mice. RGC axons from ipsilateral and contralateral eyes were labeled with β-cholera toxin conjugated to Alexa Fluor 594 (red) and Alexa Fluor 488 (green), respectively. Images of ipsilateral (***C***, ***D***) and contralateral (***E***, ***F***) projections are also shown in isolation. ***G–J***, Coronal sections through dLGN of WT (***G***, ***I***) and $Crx^{-/-}$ (***H***, ***J***) mice in which neuronal cell bodies are stained with NeuroTrace (***G***, ***H***, in magenta), and projections of posterior motion-selective DSGCs are labeled by transgenic expression of EGFP (***G***, ***H***, in green). In ***I*** and ***J***, DGSG projections are shown in isolation. ***K***, Mean ± SEM variance of *R* value distributions from β-cholera toxin injections in WT (white bars) and $Crx^{-/-}$ (red bars) mice. ***L***, Laminar targeting of *DRD4–EGFP*-expressing DSGCs is illustrated by plotting the distribution of fluorescence intensity along the width of the dLGN in WT (black line, open circles, $n = 5$ dLGNs) and $Crx^{-/-}$ (red line, filled circles, $n = 5$ dLGNs) mice.

synapses (Verhage et al., 2000; Bouwman et al., 2004; Ultanir et al., 2007; Kerschensteiner et al., 2009). This suggests that normal activity is required for normal synaptogenesis. However, whether elevated spontaneous activity is sufficient to promote synaptogenesis beyond normal levels remained unclear. Overexpression of the vesicle-associated protein synapsin IIb had been shown to advance the maturation of synapses among cultured neuroblastoma cells (Han et al., 1991), but how this result related to developing circuits *in vivo* was unknown. We find that enhanced neurotransmission in $Crx^{-/-}$ mice elevates the density of BC–RGC synapses above the norm (Fig. 7), supporting the notion that spontaneous activity in this circuit regulates synaptogenesis in a continuous, bidirectional manner. Because of its presynaptic origin (Fig. 4), the observed RGC hyperactivity cannot in turn be explained by increased BC–RGC synaptogenesis.

BCs in $Crx^{-/-}$ mice show increased spontaneous activity but lack all light responses. We interpret the changes in synaptogenesis to be caused by the increase in spontaneous rather than the absence of light-evoked activity, because they are opposite to those observed in tetanus toxin-expressing retinas in which both spontaneous and evoked glutamate release from BCs are similarly reduced (Kerschensteiner et al., 2009). A dominant role for spontaneous over visually evoked activity during BC–RGC synaptogenesis is consistent with a previous study that found the density of ribbon synapses in the IPL to be indistinguishable between dark-reared and control mice (Fisher, 1979a). However, dark rearing has been shown to cause a number of physiologic changes in the connections between BCs and RGCs (Tian and Copenhagen, 2001; Di Marco et al., 2009).

The relative influence of spontaneous and evoked activity on synaptic development varies among visual system circuits, in part because of the distinct timing of critical periods (Katz and Shatz, 1996; Hensch, 2004). For tetanus toxin-expressing BCs, synaptogenesis is reduced after P7 (Kerschensteiner et al., 2009). In $Crx^{-/-}$ mice, increased spontaneous activity from P15 onward increases synaptogenesis until P25 (Fig. 7) but not thereafter (Fig. 11). Together, these studies suggest that in mice the critical period for synaptic refinement in the inner retina extends approximately from the end of the first to the fourth week of postnatal life, when the majority of connections are established (Fisher, 1979b; Morgan et al., 2008).

Neurotransmission selectively regulates BC–RGC synapse formation, not elimination

In most developing circuits, synaptogenesis is a high turnover process in which synapse formation and elimination coexist as precise patterns of connectivity emerge (Alsina et al., 2001; Niell et al., 2004). In BC–RGC circuits, we found previously that reducing glutamate release from BCs selectively lowers the rate of synapse formation (Kerschensteiner et al., 2009) and report here that increases in spontaneous activity selectively increase this rate (Fig. 8). Neither manipulation affected synapse elimination. Sim-

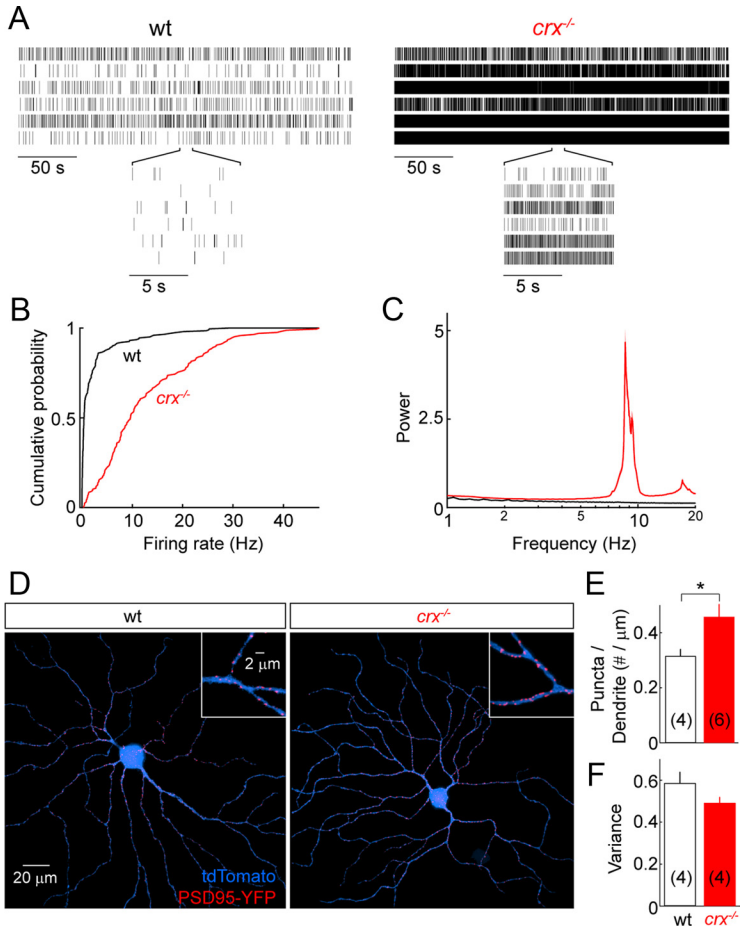

Figure 11. Retinal connectivity and retinogeniculate projections patterns stabilize despite additional hyperactivity in older $Crx^{-/-}$ mice. ***A***, Raster plots (on 2 timescales) of the spike trains of six simultaneously recorded representative RGCs in 6-month-old WT (left column) and $Crx^{-/-}$ (right column) mice. ***B***, Cumulative distributions of average RGC firing rates in 4- to 6-month-old WT (black lines) and $Crx^{-/-}$ (red lines) mice (WT, $n = 201$ cells; $Crx^{-/-}$, $n = 167$ cells). ***C***, Power spectra of RGC spike trains normalized to the peak power of the P21 $Crx^{-/-}$ dataset (Fig. 3*B*). Lines (shaded areas) represent mean ± SEM of the respective populations (WT, black; $Crx^{-/-}$, red). ***D***, Representative maximum intensity *z*-projections of confocal image stacks from RGCs biolistically labeled with tdTomato (blue) and PSD95–YFP (red) in 6-month-old WT (left) and $Crx^{-/-}$ (right) mice. Insets show higher-magnification views of excerpts from the *z*-projections. ***E***, Population data (mean ± SEM) of the density of BC synapses on RGC dendrites. The number of cells included in the analysis is shown in parentheses. *$p < 0.05$. ***F***, Mean ± SEM variance of *R* value distributions from β-cholera toxin injections in 4- to 6-month-old WT (white bars) and $Crx^{-/-}$ (red bars) mice.

cadherin-9 is required for the differentiation of mossy fiber synapses from dentate gyrus inputs (Williams et al., 2011). Activity-dependent and -independent cues likely interact throughout the nervous system not only to determine which cells connect (Cline, 2003) but also to shape the architecture of these connections.

$Crx^{-/-}$ mice are a model of LCA. Previously, large-scale circuit remodeling at late stages of this and other photoreceptor degenerative diseases had been noted (Marc et al., 2003). The changes in circuit development we report here are an important addition to these studies because, unless addressed therapeutically, they may limit the degree to which normal RGC light responses can be restored even by early replacement or photosensitization of upstream circuit elements (MacLaren et al., 2006; Lagali et al., 2008; Busskamp et al., 2010).

Normal IPL lamination and neuronal mosaics in $Crx^{-/-}$ retinas

In agreement with a previous study (Pignatelli et al., 2004), we found that BC axons and AC neurites in $Crx^{-/-}$ mice target correct sublaminae in the mature (P21) IPL (Fig. 5). In addition, both lateral branching and stratification patterns of RGC dendrites develop normally despite abnormal PR input and spontaneous activity (Fig. 7). To what extent neural activity regulates IPL lamination has been debated for some time and appears to depend on the cell type and species studied (Bodnarenko and Chalupa, 1993; Tian and Copenhagen, 2003; Stacy et al., 2005; Kerschensteiner et al., 2009; Kim et al., 2010; Xu et al., 2010). Recently, cues other than activity have emerged as key regulators of laminar targeting in the mouse IPL (Yamagata et al., 2002; Yamagata and Sanes, 2008; Matsuoka et al., 2011a,b).

Repulsive homotypic interactions, mediated in part by Down syndrome cell adhesion molecule DSCAM and DSCAM-like 1, are required for the formation of neuronal mosaics in the retina (Fuerst et al., 2008, 2009). Whether activity regulates the number and distribution of neurons in the retina is incompletely understood (Zhang et al., 2005; Anishchenko et al., 2010). Our results (Fig. 6) suggest that spontaneous and light-evoked activity play only a minor role in the organization of retinal mosaics of cholinergic ACs and DSGCs.

Maintained segregation and laminar targeting of RGC axons despite abnormal activity

Spontaneous activity of RGCs can regulate the maintenance of projection patterns of their axons in subcortical visual nuclei. When RGC activity is blocked after eye-specific territories in ferret dLGNs have been established, axons from both eyes come to overlap again (Chapman, 2000). Similarly, in *nob* mice, eye-specific territories desegregate as RGCs become hyperactive at

ilarly, local LTP induction on pyramidal neurons in hippocampal slice cultures specifically increases the rate of spine formation, without affecting the probability of spine loss (Engert and Bonhoeffer, 1999). Thus, it seems that, in circuits of the CNS, presynaptic transmitter release can promote the assembly of postsynaptic specializations. The degree to which this regulation extends to their stability likely depends on the specific circuit studied (Holtmaat et al., 2005; Zuo et al., 2005).

Neurotransmission promotes the maturation of specific connectivity patterns in a cell-type-dependent manner

By reconstructing the connectivity patterns of identified BC–RGC pairs in retinas with increased (Fig. 9) and reduced (Morgan et al., 2011) spontaneous activity, we have found that neurotransmission selectively regulates the formation of multisynaptic appositions between B6 BCs and G10 RGCs but does not affect the maintenance of connections between B7 BCs and G10 RGCs or the elimination of synapses from RB BCs. Similar cell-type-dependent regulation of synaptic maturation was described recently for the inputs to CA3 pyramidal neurons, in which

approximately P12 (Demas et al., 2006). In contrast, in $Crx^{-/-}$ mice, in which RGCs develop comparable elevated oscillatory firing at approximately P15, eye-specific dLGN territories remain intact (Fig. 10). RGCs in $Crx^{-/-}$ fire at higher rates than in *nob* mice (P21: $Crx^{-/-}$, ~5 Hz; *nob*, ~2 Hz), and their activity propagates in a wave-like manner in *nob* but not $Crx^{-/-}$ mice (Demas et al., 2006). This may indicate that not hyperactivity per se but specific patterns of RGC activity are disruptive to eye-specific segregation, a notion supported by the observation that high-frequency firing of RGCs earlier during development of $Cx36^{-/-}$ mice does not affect the formation of eye-specific territories (Torborg et al., 2005). Alternatively, the onset of hyperactivity in *nob* but not $Crx^{-/-}$ mice may fall within a period when retinogeniculate circuits are amenable to activity-dependent rewiring (Hensch, 2004). This would imply that the respective critical period closes between P12 and P15. Two lines of evidence corroborate this timing. First, in *nob* mice, most of the desegregation occurs between P12 and P14, whereas differences in the activity patterns of WT and *nob* RGCs become more pronounced later (Demas et al., 2006). Second, in a recent study, synchronous optogenetic stimulation of RGCs from both eyes led to desegregation of their axonal projections to superior colliculus only when stimuli were presented before P14 (Zhang et al., 2012).

We also show that cell-type-specific laminar targeting of DSGC axons in the dLGN is preserved despite retinal hyperactivity (Fig. 10). Together with the observation that lamination patterns of axons from another RGC type develop normally when cholinergic waves are disrupted (Huberman et al., 2008b), this indicates that cell-type-specific layers in the dLGN of mice can form and be maintained independent of retinal activity patterns.

References

Alsina B, Vu T, Cohen-Cory S (2001) Visualizing synapse formation in arborizing optic axons in vivo: dynamics and modulation by BDNF. Nat Neurosci 4:1093–1101.

Anishchenko A, Greschner M, Elstrott J, Sher A, Litke AM, Feller MB, Chichilnisky EJ (2010) Receptive field mosaics of retinal ganglion cells are established without visual experience. J Neurophysiol 103:1856–1864.

Balice-Gordon RJ, Lichtman JW (1994) Long-term synapse loss induced by focal blockade of postsynaptic receptors. Nature 372:519–524.

Blankenship AG, Feller MB (2010) Mechanisms underlying spontaneous patterned activity in developing neural circuits. Nat Rev Neurosci 11:18–29.

Blankenship AG, Ford KJ, Johnson J, Seal RP, Edwards RH, Copenhagen DR, Feller MB (2009) Synaptic and extrasynaptic factors governing glutamatergic retinal waves. Neuron 62:230–241.

Bleckert A, Wong RO (2011) Identifying roles for neurotransmission in circuit assembly: insights gained from multiple model systems and experimental approaches. Bioessays 33:61–72.

Bodnarenko SR, Chalupa LM (1993) Stratification of ON and OFF ganglion cell dendrites depends on glutamate-mediated afferent activity in the developing retina. Nature 364:144–146.

Borowska J, Trenholm S, Awatramani GB (2011) An intrinsic neural oscillator in the degenerating mouse retina. J Neurosci 31:5000–5012.

Bouwman J, Maia AS, Camoletto PG, Posthuma G, Roubos EW, Oorschot VM, Klumperman J, Verhage M (2004) Quantification of synapse formation and maintenance in vivo in the absence of synaptic release. Neuroscience 126:115–126.

Buffelli M, Burgess RW, Feng G, Lobe CG, Lichtman JW, Sanes JR (2003) Genetic evidence that relative synaptic efficacy biases the outcome of synaptic competition. Nature 424:430–434.

Busskamp V, Duebel J, Balya D, Fradot M, Viney TJ, Siegert S, Groner AC, Cabuy E, Forster V, Seeliger M, Biel M, Humphries P, Paques M, Mohand-Said S, Trono D, Deisseroth K, Sahel JA, Picaud S, Roska B (2010) Genetic reactivation of cone photoreceptors restores visual responses in retinitis pigmentosa. Science 329:413–417.

Chapman B (2000) Necessity for afferent activity to maintain eye-specific segregation in ferret lateral geniculate nucleus. Science 287:2479–2482.

Claes E, Seeliger M, Michalakis S, Biel M, Humphries P, Haverkamp S (2004) Morphological characterization of the retina of the CNGA3(−/−)Rho(−/−) mutant mouse lacking functional cones and rods. Invest Ophthalmol Vis Sci 45:2039–2048.

Cline H (2003) Sperry and Hebb: oil and vinegar? Trends Neurosci 26:655–661.

Coombs JL, Van Der List D, Chalupa LM (2007) Morphological properties of mouse retinal ganglion cells during postnatal development. J Comp Neurol 503:803–814.

Damji KF, Sohocki MM, Khan R, Gupta SK, Rahim M, Loyer M, Hussein N, Karim N, Ladak SS, Jamal A, Bulman D, Koenekoop RK (2001) Leber's congenital amaurosis with anterior keratoconus in Pakistani families is caused by the Trp278X mutation in the AIPL1 gene on 17p. Can J Ophthalmol 36:252–259.

Demas J, Eglen SJ, Wong RO (2003) Developmental loss of synchronous spontaneous activity in the mouse retina is independent of visual experience. J Neurosci 23:2851–2860.

Demas J, Sagdullaev BT, Green E, Jaubert-Miazza L, McCall MA, Gregg RG, Wong RO, Guido W (2006) Failure to maintain eye-specific segregation in nob, a mutant with abnormally patterned retinal activity. Neuron 50:247–259.

Di Marco S, Nguyen VA, Bisti S, Protti DA (2009) Permanent functional reorganization of retinal circuits induced by early long-term visual deprivation. J Neurosci 29:13691–13701.

Dubin MW, Stark LA, Archer SM (1986) A role for action-potential activity in the development of neuronal connections in the kitten retinogeniculate pathway. J Neurosci 6:1021–1036.

Engert F, Bonhoeffer T (1999) Dendritic spine changes associated with hippocampal long-term synaptic plasticity. Nature 399:66–70.

Feller MB, Wellis DP, Stellwagen D, Werblin FS, Shatz CJ (1996) Requirement for cholinergic synaptic transmission in the propagation of spontaneous retinal waves. Science 272:1182–1187.

Fisher LJ (1979a) Development of retinal synaptic arrays in the inner plexiform layer of dark-reared mice. J Embryol Exp Morphol 54:219–227.

Fisher LJ (1979b) Development of synaptic arrays in the inner plexiform layer of neonatal mouse retina. J Comp Neurol 187:359–372.

Fuerst PG, Koizumi A, Masland RH, Burgess RW (2008) Neurite arborization and mosaic spacing in the mouse retina require DSCAM. Nature 451:470–474.

Fuerst PG, Bruce F, Tian M, Wei W, Elstrott J, Feller MB, Erskine L, Singer JH, Burgess RW (2009) DSCAM and DSCAML1 function in self-avoidance in multiple cell types in the developing mouse retina. Neuron 64:484–497.

Furukawa T, Morrow EM, Cepko CL (1997) Crx, a novel otx-like homeobox gene, shows photoreceptor-specific expression and regulates photoreceptor differentiation. Cell 91:531–541.

Furukawa T, Morrow EM, Li T, Davis FC, Cepko CL (1999) Retinopathy and attenuated circadian entrainment in Crx-deficient mice. Nat Genet 23:466–470.

Ghosh KK, Bujan S, Haverkamp S, Feigenspan A, Wässle H (2004) Types of bipolar cells in the mouse retina. J Comp Neurol 469:70–82.

Han HQ, Nichols RA, Rubin MR, Bähler M, Greengard P (1991) Induction of formation of presynaptic terminals in neuroblastoma cells by synapsin IIb. Nature 349:697–700.

Hensch TK (2004) Critical period regulation. Annu Rev Neurosci 27:549–579.

Holtmaat AJ, Trachtenberg JT, Wilbrecht L, Shepherd GM, Zhang X, Knott GW, Svoboda K (2005) Transient and persistent dendritic spines in the neocortex in vivo. Neuron 45:279–291.

Huberman AD, Feller MB, Chapman B (2008a) Mechanisms underlying development of visual maps and receptive fields. Annu Rev Neurosci 31:479–509.

Huberman AD, Manu M, Koch SM, Susman MW, Lutz AB, Ullian EM, Baccus SA, Barres BA (2008b) Architecture and activity-mediated refinement of axonal projections from a mosaic of genetically identified retinal ganglion cells. Neuron 59:425–438.

Huberman AD, Wei W, Elstrott J, Stafford BK, Feller MB, Barres BA (2009) Genetic identification of an On-Off direction-selective retinal ganglion cell subtype reveals a layer-specific subcortical map of posterior motion. Neuron 62:327–334.

Jakobs TC, Koizumi A, Masland RH (2008) The spatial distribution of glu-

tamatergic inputs to dendrites of retinal ganglion cells. J Comp Neurol 510:221–236.
Katz LC, Shatz CJ (1996) Synaptic activity and the construction of cortical circuits. Science 274:1133–1138.
Kerschensteiner D, Wong RO (2008) A precisely timed asynchronous pattern of ON and OFF retinal ganglion cell activity during propagation of retinal waves. Neuron 58:851–858.
Kerschensteiner D, Liu H, Cheng CW, Demas J, Cheng SH, Hui CC, Chow RL, Wong RO (2008) Genetic control of circuit function: Vsx1 and Irx5 transcription factors regulate contrast adaptation in the mouse retina. J Neurosci 28:2342–2352.
Kerschensteiner D, Morgan JL, Parker ED, Lewis RM, Wong RO (2009) Neurotransmission selectively regulates synapse formation in parallel circuits in vivo. Nature 460:1016–1020.
Kim IJ, Zhang Y, Meister M, Sanes JR (2010) Laminar restriction of retinal ganglion cell dendrites and axons: subtype-specific developmental patterns revealed with transgenic markers. J Neurosci 30:1452–1462.
Lagali PS, Balya D, Awatramani GB, Münch TA, Kim DS, Busskamp V, Cepko CL, Roska B (2008) Light-activated channels targeted to ON bipolar cells restore visual function in retinal degeneration. Nat Neurosci 11:667–675.
Lee EJ, Merwine DK, Padilla M, Grzywacz NM (2007) Choline acetyltransferase-immunoreactive neurons in the retina of normal and dark-reared turtle. J Comp Neurol 503:768–778.
MacLaren RE, Pearson RA, MacNeil A, Douglas RH, Salt TE, Akimoto M, Swaroop A, Sowden JC, Ali RR (2006) Retinal repair by transplantation of photoreceptor precursors. Nature 444:203–207.
Marc RE, Jones BW, Watt CB, Strettoi E (2003) Neural remodeling in retinal degeneration. Prog Retin Eye Res 22:607–655.
Margolis DJ, Detwiler PB (2011) Cellular origin of spontaneous ganglion cell spike activity in animal models of retinitis pigmentosa. J Ophthalmol 2011:pii:507037.
Margolis DJ, Newkirk G, Euler T, Detwiler PB (2008) Functional stability of retinal ganglion cells after degeneration-induced changes in synaptic input. J Neurosci 28:6526–6536.
Masland RH (2001) The fundamental plan of the retina. Nat Neurosci 4:877–886.
Matsuoka RL, Nguyen-Ba-Charvet KT, Parray A, Badea TC, Chédotal A, Kolodkin AL (2011a) Transmembrane semaphorin signalling controls laminar stratification in the mammalian retina. Nature 470:259–263.
Matsuoka RL, Chivatakarn O, Badea TC, Samuels IS, Cahill H, Katayama K, Kumar SR, Suto F, Chédotal A, Peachey NS, Nathans J, Yoshida Y, Giger RJ, Kolodkin AL (2011b) Class 5 transmembrane semaphorins control selective mammalian retinal lamination and function. Neuron 71:460–473.
Morgan JL, Kerschensteiner D (2011) Shooting DNA, dyes, or indicators into tissue slices using the gene gun. Cold Spring Harb Protoc 2011:1512–1514.
Morgan JL, Kerschensteiner D (2012) Coating gold particles with DNA (biolistics). Cold Spring Harb Protoc 2012:114–117.
Morgan JL, Schubert T, Wong RO (2008) Developmental patterning of glutamatergic synapses onto retinal ganglion cells. Neural Dev 3:8.
Morgan JL, Soto F, Wong RO, Kerschensteiner D (2011) Development of cell type-specific connectivity patterns of converging excitatory axons in the retina. Neuron 71:1014–1021.
Morrow EM, Furukawa T, Raviola E, Cepko CL (2005) Synaptogenesis and outer segment formation are perturbed in the neural retina of Crx mutant mice. BMC Neurosci 6:5.
Niell CM, Meyer MP, Smith SJ (2004) In vivo imaging of synapse formation on a growing dendritic arbor. Nat Neurosci 7:254–260.
Okabe S, Kim HD, Miwa A, Kuriu T, Okado H (1999) Continual remodeling of postsynaptic density and its regulation by synaptic activity. Nat Neurosci 2:804–811.
Otsu N (1979) A threshold selection method from gray-level histograms. IEEE Trans Syst Man Cybern 9:62–66.
Penn AA, Riquelme PA, Feller MB, Shatz CJ (1998) Competition in retinogeniculate patterning driven by spontaneous activity. Science 279:2108–2112.
Pfeiffenberger C, Cutforth T, Woods G, Yamada J, Rentería RC, Copenhagen DR, Flanagan JG, Feldheim DA (2005) Ephrin-As and neural activity are required for eye-specific patterning during retinogeniculate mapping. Nat Neurosci 8:1022–1027.
Pignatelli V, Cepko CL, Strettoi E (2004) Inner retinal abnormalities in a mouse model of Leber's congenital amaurosis. J Comp Neurol 469:351–359.
Rodieck RW (1991) The density recovery profile: a method for the analysis of points in the plane applicable to retinal studies. Vis Neurosci 6:95–111.
Soto F, Bleckert A, Lewis R, Kang Y, Kerschensteiner D, Craig AM, Wong RO (2011) Coordinated increase in inhibitory and excitatory synapses onto retinal ganglion cells during development. Neural Dev 6:31.
Stacy RC, Demas J, Burgess RW, Sanes JR, Wong RO (2005) Disruption and recovery of patterned retinal activity in the absence of acetylcholine. J Neurosci 25:9347–9357.
Stasheff SF (2008) Emergence of sustained spontaneous hyperactivity and temporary preservation of OFF responses in ganglion cells of the retinal degeneration (rd1) mouse. J Neurophysiol 99:1408–1421.
Tian N, Copenhagen DR (2001) Visual deprivation alters development of synaptic function in inner retina after eye opening. Neuron 32:439–449.
Tian N, Copenhagen DR (2003) Visual stimulation is required for refinement of ON and OFF pathways in postnatal retina. Neuron 39:85–96.
Torborg CL, Feller MB (2004) Unbiased analysis of bulk axonal segregation patterns. J Neurosci Methods 135:17–26.
Torborg CL, Hansen KA, Feller MB (2005) High frequency, synchronized bursting drives eye-specific segregation of retinogeniculate projections. Nat Neurosci 8:72–78.
Ultanir SK, Kim JE, Hall BJ, Deerinck T, Ellisman M, Ghosh A (2007) Regulation of spine morphology and spine density by NMDA receptor signaling in vivo. Proc Natl Acad Sci U S A 104:19553–19558.
Verhage M, Maia AS, Plomp JJ, Brussaard AB, Heeroma JH, Vermeer H, Toonen RF, Hammer RE, van den Berg TK, Missler M, Geuze HJ, Südhof TC (2000) Synaptic assembly of the brain in the absence of neurotransmitter secretion. Science 287:864–869.
Völgyi B, Chheda S, Bloomfield SA (2009) Tracer coupling patterns of the ganglion cell subtypes in the mouse retina. J Comp Neurol 512:664–687.
Wässle H (2004) Parallel processing in the mammalian retina. Nat Rev Neurosci 5:747–757.
Wässle H, Puller C, Müller F, Haverkamp S (2009) Cone contacts, mosaics, and territories of bipolar cells in the mouse retina. J Neurosci 29:106–117.
Williams ME, Wilke SA, Daggett A, Davis E, Otto S, Ravi D, Ripley B, Bushong EA, Ellisman MH, Klein G, Ghosh A (2011) Cadherin-9 regulates synapse-specific differentiation in the developing hippocampus. Neuron 71:640–655.
Wong RO (1999) Retinal waves and visual system development. Annu Rev Neurosci 22:29–47.
Wong RO, Meister M, Shatz CJ (1993) Transient period of correlated bursting activity during development of the mammalian retina. Neuron 11:923–938.
Xu HP, Chen H, Ding Q, Xie ZH, Chen L, Diao L, Wang P, Gan L, Crair MC, Tian N (2010) The immune protein CD3zeta is required for normal development of neural circuits in the retina. Neuron 65:503–515.
Yamagata M, Sanes JR (2008) Dscam and Sidekick proteins direct lamina-specific synaptic connections in vertebrate retina. Nature 451:465–469.
Yamagata M, Weiner JA, Sanes JR (2002) Sidekicks: synaptic adhesion molecules that promote lamina-specific connectivity in the retina. Cell 110:649–660.
Zhang J, Yang Z, Wu SM (2005) Development of cholinergic amacrine cells is visual activity-dependent in the postnatal mouse retina. J Comp Neurol 484:331–343.
Zhang J, Ackman JB, Xu HP, Crair MC (2012) Visual map development depends on the temporal pattern of binocular activity in mice. Nat Neurosci 15:298–307.
Zheng J, Lee S, Zhou ZJ (2006) A transient network of intrinsically bursting starburst cells underlies the generation of retinal waves. Nat Neurosci 9:363–371.
Zuo Y, Yang G, Kwon E, Gan WB (2005) Long-term sensory deprivation prevents dendritic spine loss in primary somatosensory cortex. Nature 436:261–265.